C.N.R.S.
Centre National de la Recherche Scientifique

I.N.F.N.
Instituto Nazionale di Fisica Nucleare

Analysis of the sensitivity of the recombined interferometer during C4 and C5 runs

R. Flaminio, R. Gouaty, E. Tournefier

VIR-NOT-LAP-1390-312

Issue 1
Date: 15th January 2006

VIRGO * A joint CNRS-INFN Project
Project office: Traversa H di via Macerata - I-56021 S. Stefano a Macerata, Cascina (PI)
Secretariat: Telephone (39) 50 752 521 – Fax (39) 50 752 550 – e-mail virgo@pisa.infn.it

Contents

1 Introduction **3**

2 The C4 and C5 commissioning runs **3**

3 The common mode rejection factor **5**
3.1 Impact of an asymmetry between the two arms: general computation . . . 6
3.2 Asymmetry of the finesses . . . 7
3.3 Asymmetry of the reflectivity modulus . . . 10
3.3.1 Asymmetry of the end mirrors radius of curvature . . . 11
3.3.2 Asymmetry in the beam splitter . . . 12
3.4 Asymmetry of the cavity losses . . . 13

4 Analysis of the C4 run sensitivity **14**
4.1 Dark fringe readout noise . . . 15
4.2 Laser frequency noise . . . 15
4.3 Actuator noise . . . 17
4.4 Beam splitter control noises . . . 21
4.4.1 Contribution of the BS control noises in sensitivity . . . 21
4.4.2 Analytical models for the propagation of BS control noises . . . 24
4.4.3 Origin of the noise in the BS longitudinal control loop . . . 27
4.5 Noise budget of the C4 run . . . 31

5 Analysis of the C5 run sensitivity **31**
5.1 Dark fringe readout and laser frequency noise . . . 32
5.2 Actuator noise . . . 33
5.3 Beam splitter control noises . . . 35
5.4 Noise budget of the C5 run . . . 35

6 Conclusion **35**

A Effect of an asymmetry between the two cavities in the recombined configuration **37**

1 Introduction

In 2004 the Virgo interferometer was run several times in the so-called recombined configuration. In this configuration each of the two arm cavities is kept aligned and locked to the resonance of the TEM_{00} mode in order to obtain an interference between the two reflected beams. Moreover this interference is locked to the dark fringe. The recombined configuration was first tested for 24 hours during the C3 commissioning run from April 26th to April 27th, 2004, using a temporary locking strategy. During the following run (C4) it was possible to collect a five days long set of data (from June 24th to June 29th of 2004) in the recombined configuration using the final locking strategy. At the end of 2004 the C5 run allowed another data taking (from December 2nd to December 7th of 2004) in a configuration similar to C4 but including the so-called suspension hierarchical control as well as other technical upgrades.

The goal of this note is to list the dominant noise sources which have an impact on the recombined interferometer sensitivity. The analysis is focused on C4 and C5 runs for which the control strategy had reached a stable state. The locking scheme is presented in section 2 as well as the sensivitity curves obtained during the C4 and C5 runs. The properties of the interferometer common mode rejection factor, which explain most of the improvement observed in the recombined interferometer sensitivity with respect to the Fabry-Perot configuration, are discussed in section 3. The noise sources limiting the C4 and C5 sensitivities are described in sections 4 and 5 respectively.

2 The C4 and C5 commissioning runs

The locking scheme used for both C4 and C5 runs is shown in Figure 1. In the recombined configuration three longitudinal degrees of freedom have to be controlled: the Fabry Perot differential mode, the short Michelson differential mode, and the Fabry Perot common mode which is equivalent to a laser frequency variation. The locking strategy which has been choosen is the following:

- The Fabry Perot length asymmetry, called differential mode, is controlled by sending opposite corrections to the end mirrors. These corrections are computed from the dark fringe signal ($B1\_ACp$) which is sensitive to differential motions.
- The length asymmetry of the short michelson is controlled by acting on the beam splitter mirror. This loop uses the $B2\_ACq$ signal (provided by the photodiode which receives the interferometer reflection) as error signal.
- The laser frequency is controlled by an analog loop using the $B2\_ACp$ signal which is sensitive to the common length fluctuations of the Fabry-Perot cavities. An additional loop sends corrections to the end mirrors to control the common mode at low frequencies (the unity gain frequency is around 2 Hz). This loop uses as error signal the reflection of the reference cavity, which is sensitive to laser frequency fluctuations.

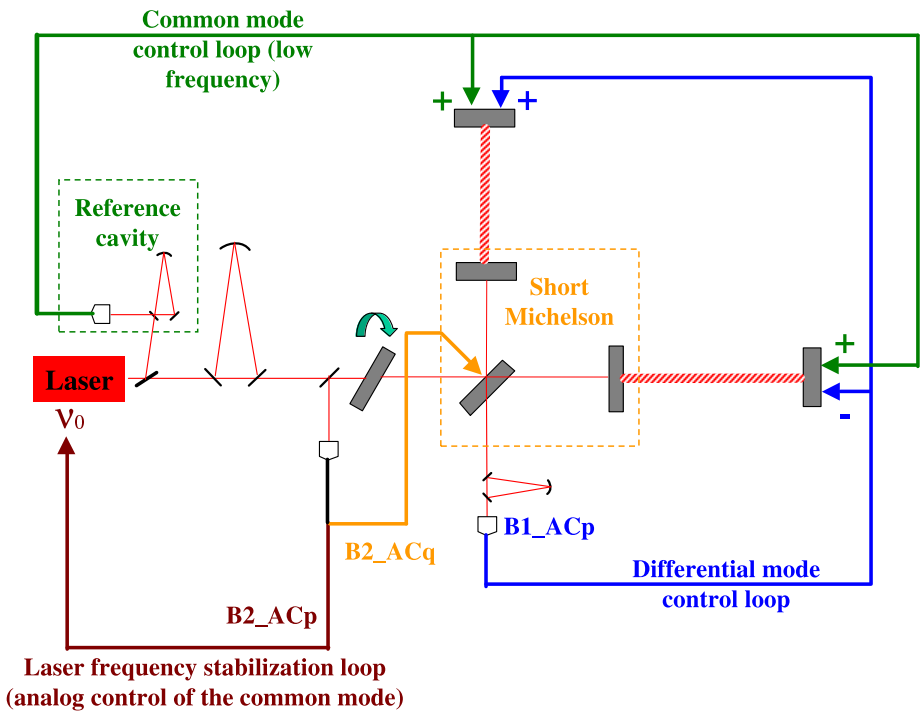

Figure 1: *The recombined locking scheme (for legibility reasons the intput mode cleaner control loops have been omitted).*

During the C4 run the locking correction forces were directly applied to the mirrors by sending a current in the reference mass coils. During the C5 run it was tested a more sophisticated actuation strategy, called hierarchical control. This consists in splitting the correction force between the marionette and the reference mass. The low frequency correction forces are applied to the marionettes whereas the high frequency correction forces are still applied to the mirrors. The crossover between these two actuation methods is typically around a few Hertz. The advantage of such a strategy regarding the introduction of actuation noise will be explained in section 5.

For what concerns the angular degrees of freedom, the arm mirrors were under linear alignment during both C4 and C5 runs, and the beam splitter mirror was under local control.

The C4 and C5 sensitivities (shown in Figure 2) are analysed in the following sections. One can already notice that the C5 sensitivity is worse in the high frequency region with respect to the C4 sensitivity. This is due to the change in the optical setup of the injection bench which decreases the power entering the interferometer by a factor 10 (0.8 W for C5 instead of 8 W for C4). This temporary modification has been performed in order to attenuate the effect of some diffused light in the injection bench.

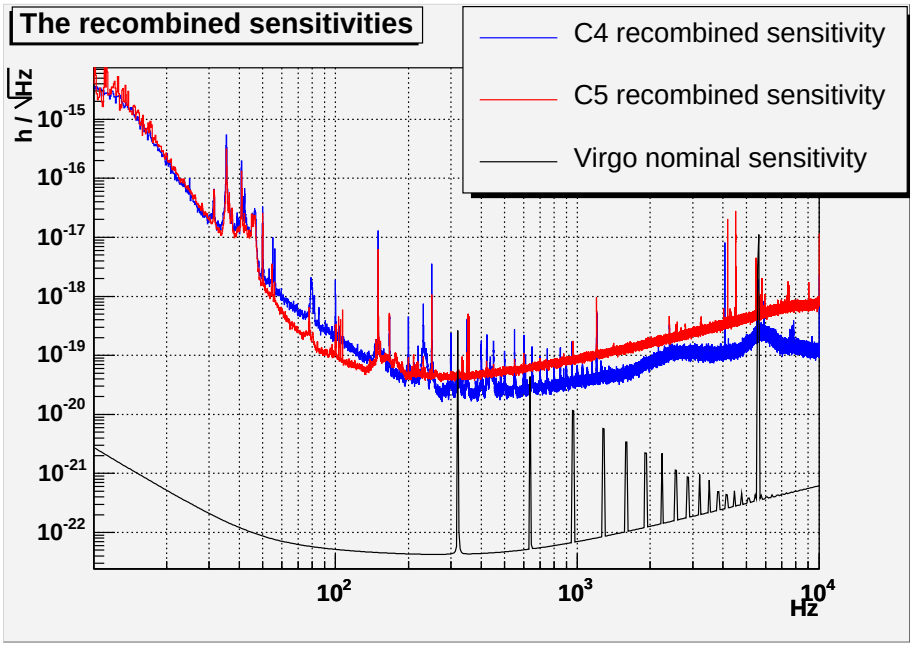

Figure 2: *The recombined sensitivities (C4 and C5 runs) compared to the Virgo nominal sensitivity*

3 The common mode rejection factor

In the recombined configuration the beam reflected by one arm interferes destructively with the beam reflected by the other thus cancelling the impact of the laser frequency noise (and more generally of every common mode noise) on the interferometer sensitivity. This cancellation is not perfect due to asymetries between the two arms. The attenuation factor, which is a priori frequency dependant, is called the Common Mode Rejection Factor (CMRF) and is defined as:

$$CMRF \;=\; \left|\left|\frac{\delta\tilde{l}/L}{\delta\tilde{\nu}/\nu}\right|\right| \tag{1}$$

where L is the Fabry Perot cavity length, ν is the laser frequency, $\delta\tilde{l}$[1] refers to the difference of length between the two Fabry Perot cavities which is equivalent for the interferometer output port to the effect of the laser frequency noise $\delta\tilde{\nu}$.
Low values of the CMRF mean an efficient cancellation of the laser frequency noise. The definition of the CMRF can also be written as:

$$CMRF \;=\; \left|\left|\frac{\delta\tilde{l}}{\delta\tilde{L}}\right|\right| \tag{2}$$

with $\delta\tilde{L} \;=\; \delta\tilde{\nu}\times\frac{L}{\nu}$, $\delta\tilde{L}$ is the common mode length fluctuation of the Fabry Perot cavities which is equivalent to the laser frequency noise $\delta\tilde{\nu}$.

[1]Throughout this note the notation $\delta\tilde{X}$ refers to the fluctuation of the variable X taken in the frequency domain, while the notation δX refers to the modulus of $\delta\tilde{X}$.

The quality of the rejection of laser frequency noise is limited by the asymmetries between the two arms like difference of finesse or difference of reflectivity. A SIESTA simulation [1] of the recombined interferometer was used to examine the impact of the most significant asymmetry sources on the CMRF. The results of this analysis are presented in the following subsections.

3.1 Impact of an asymmetry between the two arms: general computation

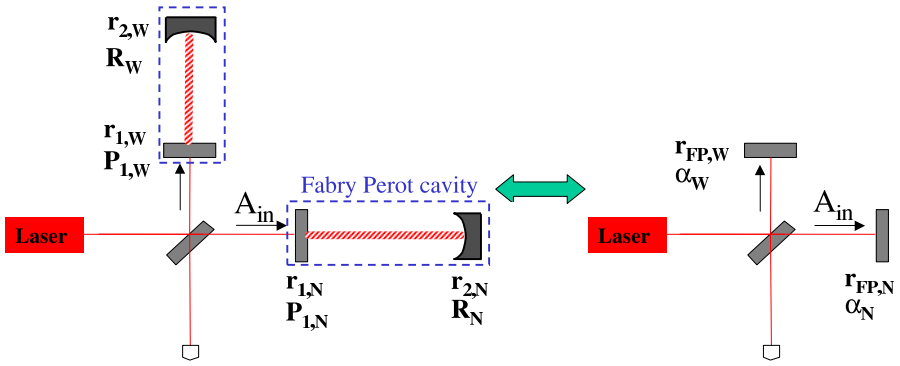

Figure 3: *Recombined interferometer with Fabry Perot cavities.*

A Fabry Perot cavity (shown in Figure 3) is seen by the incident beam as a mirror having a reflectivity r_{FP}[2]:

$$r_{FP} = -\rho_{FP} e^{i\Phi_{FP}} \tag{3}$$

For a resonant Fabry Perot cavity (as it is the case for the beam carrier), the reflectivity modulus ρ_{FP} is given by:

$$\rho_{FP} = \left| \frac{r_1 - (1 - P_1) r_2}{1 - r_1 r_2} \right| \tag{4}$$

where r_1 and r_2 are the reflectivities of the input mirror and of the end mirror respectively, P_1 refers to the losses of the input mirror.

[2]Throughout this note the reflectivities written with the notation r are field reflectivities while the loss coefficients written with the notation P are expressed in term of power

The phase response Φ_{FP} of a resonant Fabry Perot cavity to a length fluctuation δL is given in the frequency domain by:

$$\tilde{\Phi}_{FP} \;=\; \frac{4F}{\pi}\frac{2\pi}{\lambda}\frac{\delta\tilde{L}}{1+i\frac{f}{f_{cav}}} \tag{5}$$

where f is the frequency of the mirror motion, λ is the wave length of the laser, F is the finesse of the cavity, and f_{cav} is the pole of the cavity: $f_{cav} \;=\; \frac{c}{4FL}$. For frequencies higher than f_{cav}, the laser propagation time inside the cavity is not negligible so that the phase response is filtered.

The effect of an asymmetry between the two arms on the propagation of laser frequency noise to the interferometer output signal can be evaluated by computing the sensitivity of the latter to a common length variation of the two arm cavities δL. As shown in Appendix A the signal S_p obtained after the demodulation process is given by:

$$S_p \;=\; 4A^2 J_0(m) J_1(m)\sqrt{T} Re(-i\Delta r) \tag{6}$$

where:

- Δr is the difference between the reflectivities of the two Fabry Perot cavities for the carrier:

$$\Delta r \;=\; \frac{r_{FP,W} - r_{FP,N}}{2} \;=\; \frac{1}{2}\Big(\rho_{FP,N} e^{i\Phi_{FP,N}} - \rho_{FP,W} e^{i\Phi_{FP,W}}\Big) \tag{7}$$

  The indexes N and W refer to the north and west cavities respectively.

- T is the transmission factor of the side-bands.

- J_0 and J_1 refer to the Bessel functions, m is the modulation index.

- A is the amplitude of the laser beam entering the interferometer.

Different kinds of asymmetry between the two Fabry-Perot cavities are discussed in the following subsections.

3.2 Asymmetry of the finesses

The effect of an asymmetry of the finesses is considered in this subsection whereas the reflectivity modulus are supposed to be the same for both Fabry Perot cavities. The finesse of a Fabry Perot cavity is given by:

$$F \;=\; \frac{\pi\sqrt{r_1 r_2}}{1 - r_1 r_2} \tag{8}$$

According to equation (8) an asymmetry of the finesses is generated by a difference between the mirror reflectivities of the two Fabry Perot cavities. Equation (4) shows that

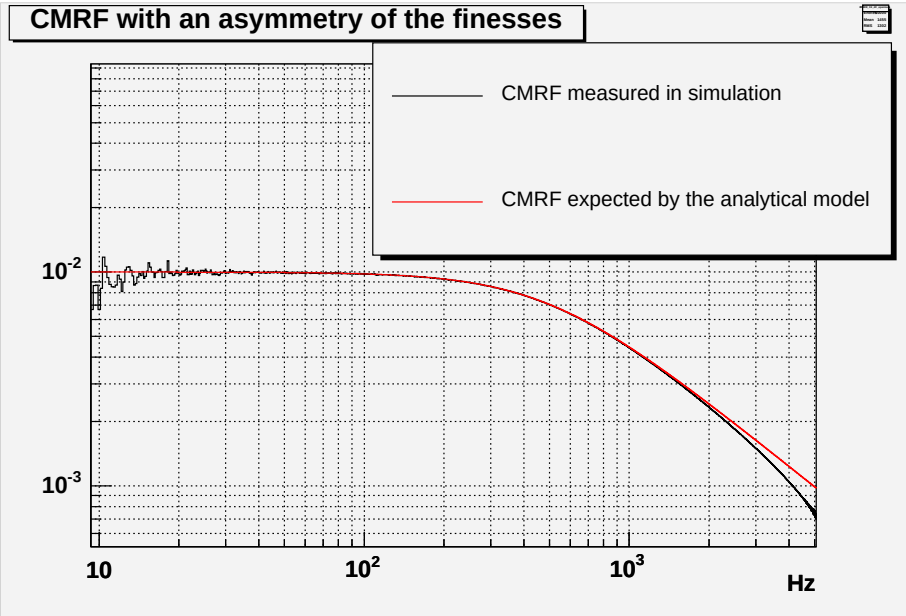

Figure 4: *CMRF due to a finesse asymmetry*

the reflectivity modulus ρ_{FP} also depends on the values of mirror reflectivities. Nevertheless if the end mirror reflectivity satisfies the condition $1 - r_2^2 << 1 - r_1$ and if the mirror losses are negligible ($P_1 << 1 - r_1$), then ρ_{FP} can be approximated by 1 for both Fabry Perot cavities. In these conditions, relation (7) simplifies into:

$$\Delta r = \frac{1}{2}\left(e^{i\Phi_{FP,N}} - e^{i\Phi_{FP,W}}\right) \approx i\frac{\Phi_{FP,N} - \Phi_{FP,W}}{2} \tag{9}$$

Relation (6) is developped using relation (9), which leads to:

$$S_p \approx 2A^2 J_0(m) J_1(m)\sqrt{T}(\Phi_{FP,N} - \Phi_{FP,W}) \tag{10}$$

The previous equation can be re-written in the frequency domain using the expression of the cavity phase response given in (5):

$$\tilde{S}_p \approx 2A^2 J_0(m) J_1(m)\sqrt{T}\frac{2\pi}{\lambda}\frac{4(F_N - F_W)}{\pi}\frac{\delta\tilde{L}}{\left(1 + i\frac{f}{f_{cav,N}}\right)\left(1 + i\frac{f}{f_{cav,W}}\right)} \tag{11}$$

The signal induced by a differential motion $\delta\tilde{l}$ of the end mirrors due to a gravitationnal wave has been computed in [2] (in this case the effect of the asymmetry of the finesses can be neglected):

$$\tilde{S}_p = 2A^2 J_0(m) J_1(m)\sqrt{T}\frac{2\pi}{\lambda}\frac{4F}{\pi}\frac{\delta\tilde{l}}{1 + i\frac{f}{f_{cav}}} \tag{12}$$

where F is the average of the finesses and f_{cav} the average of the two cavity poles. The expected CMRF due to an asymmetry of the finesses is deduced from relations (11) and (12):

$$CMRF = \left\| \frac{\delta \tilde{l}}{\delta \tilde{L}} \right\| = \frac{|F_N - F_W|}{F} \frac{1}{\sqrt{1 + \left(\frac{f}{f_{cav}}\right)^2}} \tag{13}$$

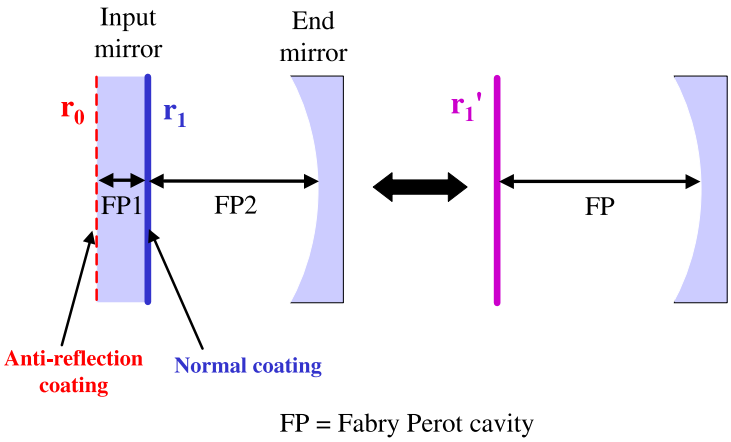

Figure 5: *Internal Fabry Perot cavity in the input mirror.*

A simulation of the recombined interferometer has been performed in order to check the previous analytical model. In this simulation the mirrors are not controlled but the seismic noise is turned off so that the dark fringe and the cavity resonance conditions are satisfied. An asymmetry of the finesses of 1% is included by choosing different values of the input mirror reflectivity for the two arms, while the mirror losses are put to zero. The mirror reflectivity values used in this simulation can be found in Table 1, they are compatible with the mirror specifications. The CMRF is measured by injecting a laser frequency noise and then computing the transfer function between the injected noise and the measured sensitivity, according to equation (1). The CMRF obtained in simulation confirms the prediction given by the analytical model as shown in Figure 4. It can be noticed that an asymmetry of the finesses has a dominant impact on the CMRF at low frequencies (up to a few hundred Hertz) due to the Fabry-Perot low-pass filtering.

For what concerns the real interferometer the finesse asymmetry is likely to vary due to the Fabry-Perot effect in the input mirrors. These mirrors have a high reflection coating that defines their reflectivity r_1 on one side, and an anti-reflection coating on the other side, as shown in Figure 5. Due to the residual reflectivity r_0 of the anti-reflection coating there is a Fabry-Perot cavity inside the input mirrors. This effect can be described by defining a global reflectivity r_1' of the input mirror which depends on the intra-mirror cavity length. The optical length of this cavity can change by several wavelengths with

	r_1	r_2	F
North cavity	0.9388	0.999976	49.75
West cavity	0.9394	0.999976	50.25

Table 1: *Values used in the simulation of a 1% finesse asymmetry.*

the temperature of the mirror, so that it can generate variations of the global reflectivity of the input mirror and, as a consequence, variations of the finesse. A computation made in [3] shows that the maximum variation of the finesse that can result from the Fabry-Perot effect in the input mirrors is:

$$\frac{\Delta F}{F} \;=\; \pm 2 r_0 \tag{14}$$

According to the measurements performed by the LMA in Lyon the reflectivity of the anti-reflection coating r_0 is such that: $r_0^2 \;\approx\; 150\; ppm$, which gives for the maximum variation of the finesse: $\frac{\Delta F}{F} \;=\; \pm 0.024$. As these variations are not correlated between the two arms, the asymmetry of the finesses can vary from 0 to about 5 %. This corresponds to a maximum CMRF of 0.05 at low frequencies. In this case the residual CMRF at 5 kHz would be about 0.005.

3.3 Asymmetry of the reflectivity modulus

The effect of an asymmetry between the two cavity reflectivity modulus ($\rho_{FP,N} \;\neq\; \rho_{FP,W}$) is now considered whereas the finesses are assumed to be the same for both Fabry Perot cavities. In these conditions the optical path lengths inside both cavities are identical, which means that the impact of this kind of asymmetry is not filtered by the cavity. As a consequence the CMRF is expected to be constant whatever frequency is considered. The difference between the reflectivities of the two cavities can be written as:

$$\Delta r \;=\; \frac{\rho_{FP,N} - \rho_{FP,W}}{2} e^{i\Phi_{FP}} \;\approx\; \frac{\rho_{FP,N} - \rho_{FP,W}}{2}(1 + i\Phi_{FP}) \tag{15}$$

The signal induced at the output port of the interferometer by a common mode noise can be deduced from relation (6) by replacing Δr by its expression given in (15):

$$S_p \;\approx\; 2A^2 J_0(m) J_1(m) \sqrt{T} (\rho_{FP,N} - \rho_{FP,W}) \Phi_{FP} \tag{16}$$

In the frequency domain relation (16) becomes:

$$\tilde{S}_p \;\approx\; 2A^2 J_0(m) J_1(m) \sqrt{T} (\rho_{FP,N} - \rho_{FP,W}) \frac{2\pi}{\lambda} \frac{4F}{\pi} \frac{\delta \tilde{L}}{1 + i\frac{f}{f_{cav}}} \tag{17}$$

The expected CMRF due to an asymmetry of the reflectivity modulus is deduced from relations (17) and (12):

$$CMRF \;=\; \left|\left| \frac{\delta \tilde{l}}{\delta \tilde{L}} \right|\right| \;=\; |\rho_{FP,N} - \rho_{FP,W}| \tag{18}$$

There are various mechanisms that can generate a difference between the reflectivity modulus of the two Fabry-Perot cavities; two of these are discussed in the following subsections.

3.3.1 Asymmetry of the end mirrors radius of curvature

An asymmetry of the reflectivity modulus can originate from an asymmetry of the radius of curvature of the end mirrors in case of a mismatching between the incident beam and the beam resonating into the Fabry Perot cavity.

The incident beam field A_{in} (shown in Figure 3) can be written as:

$$A_{in} \;=\; A_{00,in}\Psi_{00,in}(x,y) \;=\; A_{00,in}\sqrt{\frac{2}{\pi}}\frac{1}{w_{0,in}}e^{-\frac{x^2+y^2}{w_{0,in}^2}} \tag{19}$$

$A_{00,in}$ is the field amplitude, $\Psi_{00,in}$ refers to the 00 mode (TEM_{00}) of the Hermite-Gauss basis. $w_{0,in}$ is the waist of the incident beam, x and y refer to the cartesian coordinates in the plane perpendicular to the direction of propagation. Relation (19) is obtained assuming an infinite radius of curvature. The TEM_{00} mode resonating in the Fabry-Perot cavity and computed at the input of the cavity is also given by:

$$\Psi_{00,N(W)}(x,y) \;=\; \sqrt{\frac{2}{\pi}}\frac{1}{w_{0,N(W)}}e^{-\frac{x^2+y^2}{w_{0,N(W)}^2}} \tag{20}$$

The waist $w_{0,N(W)}$ depends on the radius of curvature $R_{N(W)}$ of the end mirror according to the relation:

$$w_{0,N(W)}^2 \;=\; L\frac{\lambda}{\pi}\sqrt{\frac{R_{N(W)}}{L}-1} \tag{21}$$

The matching coefficient ($\alpha_{N(W)}$) between the incident beam and the TEM_{00} mode resonating in the Fabry-Perot cavity can be obtained computing the scalar product between $\Psi_{00,in}$ and $\Psi_{00,N(W)}$ in the Hermite-Gauss basis:

$$\alpha_{N(W)} \;=\; \int_x\int_y \Psi_{00,in}(x,y)\bar{\Psi}_{00,N(W)}(x,y)\;dxdy \;=\; \frac{2\;w_{0,in}\;w_{0,N(W)}}{w_{0,in}^2+w_{0,N(W)}^2} \tag{22}$$

The amplitude of the TEM_{00} mode resonating inside the cavity is weighted by the factor $\alpha_{N(W)}$ with respect to the amplitude $A_{00,in}$ of the incident beam. The amplitude of the TEM_{00} mode reflected by the Fabry Perot cavity is again attenuated by the same factor with respect to the resonant TEM_{00} mode. Finally the Fabry Perot cavity is seen by the incident beam as a mirror having an effective reflectivity $r'_{FP,N(W)}$ given by:

$$r'_{FP,N(W)} \;=\; -\rho'_{FP,N(W)}e^{i\Phi_{FP}} \;=\; -\rho_{FP}\alpha_{N(W)}^2e^{i\Phi_{FP}} \tag{23}$$

If the radius of curvature differs from one end mirror to the other one, the difference between the matching coefficients of the two Fabry Perot cavities produces a CMRF which can be written following (18) as:

$$CMRF \;=\; \rho_{FP}|\alpha_N^2 - \alpha_W^2| \tag{24}$$

The results of a numerical computation are presented in Table 2. The radius of curvature measured for Virgo mirrors are [4]:

$$R_N \;=\; 3555 \pm 20\ m \quad and \quad R_W \;=\; 3570 \pm 40\ m \tag{25}$$

The common mode rejection factor for different values of the mirrors radius of curvature and for different level of beam matching is given in Table 2. For an incident beam waist ajusted within 3 % with the mean of the cavity waists ($w_{0,in} \;=\; 2.04 \times 10^{-2}\ m$) the CMRF is 3.7×10^{-4}. For a mismatching comparable to the situation of C4 and C5 runs for which $\alpha_{N,W}^2$ has been found around 0.95 (which corresponds to $w_{0,in} \;=\; 1.67 \times 10^{-2}\ m$), the CMRF is of the order of a few parts per thousand. This value increases to 1.4×10^{-2} if the extreme values for the end mirrors radius of curvature are considered.

Incident beam	Cavity	ROC	Cavity waist	Matching	CMRF
$w_{0,in} \;=\; 2.04 \times 10^{-2}\ m$	North	3555 m	$2.09 \times 10^{-2}\ m$	$\alpha_N^2 \approx 0.9994$	3.7×10^{-4}
	West	3570 m	$2.104 \times 10^{-2}\ m$	$\alpha_W^2 \approx 0.9990$	
$w_{0,in} \;=\; 1.67 \times 10^{-2}\ m$	North	3555 m	$2.09 \times 10^{-2}\ m$	$\alpha_N^2 \approx 0.951$	2.8×10^{-3}
	West	3570 m	$2.104 \times 10^{-2}\ m$	$\alpha_W^2 \approx 0.948$	
$w_{0,in} \;=\; 1.67 \times 10^{-2}\ m$	North	3535 m	$2.07 \times 10^{-2}\ m$	$\alpha_N^2 \approx 0.955$	1.4×10^{-2}
	West	3610 m	$2.14 \times 10^{-2}\ m$	$\alpha_W^2 \approx 0.941$	

Table 2: *Effect of an asymmetry of the radius of curvature (ROC) of the end mirrors.*

3.3.2 Asymmetry in the beam splitter

In equation (6) Δr has been defined as the difference between the reflectivities of the two Fabry Perot cavities. In fact the residual reflectivity $r_{0,BS}$ of the anti-reflection coating of the beam splitter mirror (shown in Figure 6) also generates an optical asymmetry between the two arms. This is due to the fact that the beam reflected by the north arm and reaching the semi-reflective side of the beam splitter, where is located the interference point, has crossed two times the anti-reflective side, whereas the beam reflected by the west arm never crossed it. The effect of this asymmetry is equivalent to the effect of an asymmetry of the reflectivity modulus between the two cavities and can be described by replacing equation (15) by:

$$\Delta r \;=\; (\rho_{FP,N} t_{0,BS}^2 - \rho_{FP,W}) e^{i\Phi_{FP}} \tag{26}$$

where $t_{0,BS}$ is the transmittivity of the anti-reflection coating of the beam splitter. If the losses are negligible then $t_{0,BS}$ is given by:

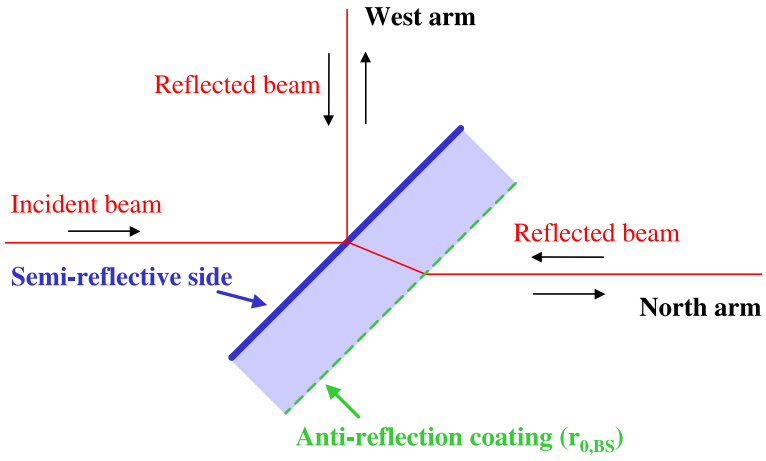

Figure 6: *The beam splitter mirror and its anti-reflection coating.*

$$t_{0,BS} \approx \sqrt{1 - r_{0,BS}^2} \tag{27}$$

If the reflectivities of the two Fabry Perot cavities are assumed to be identical, then the CMRF induced by the single contribution of the residual reflectivity of the beam splitter anti-reflection coating is given by:

$$CMRF = 1 - t_{0,BS}^2 \approx r_{0,BS}^2 \tag{28}$$

A measurement performed by the LMA in Lyon gave: $r_{0,BS}^2 = 520\,ppm$. The resulting CMRF is equal to 2.6×10^{-4}. This value is one order of magnitude lower than the one expected with an asymmetry of beam mismatching corresponding to C4 or C5 situation. Consequently this effect should be negligible.

3.4 Asymmetry of the cavity losses

A difference between the losses in the two arm cavities will also produce an asymmetry of the reflectivity modulus. This case is more complex since a difference in the losses will also produce an asymmetry between the cavity phase responses. A detailed analytical calculation shows that the second effect tends to compensate the first; the result is that the common mode rejection factor is well approximated by the expression:

$$CMRF = \frac{F}{2\pi}\Delta P \tag{29}$$

Where F is the average of the cavity finesses and ΔP is the difference between the two cavity losses. A simulation has been performed considering an asymmetry of the cavity

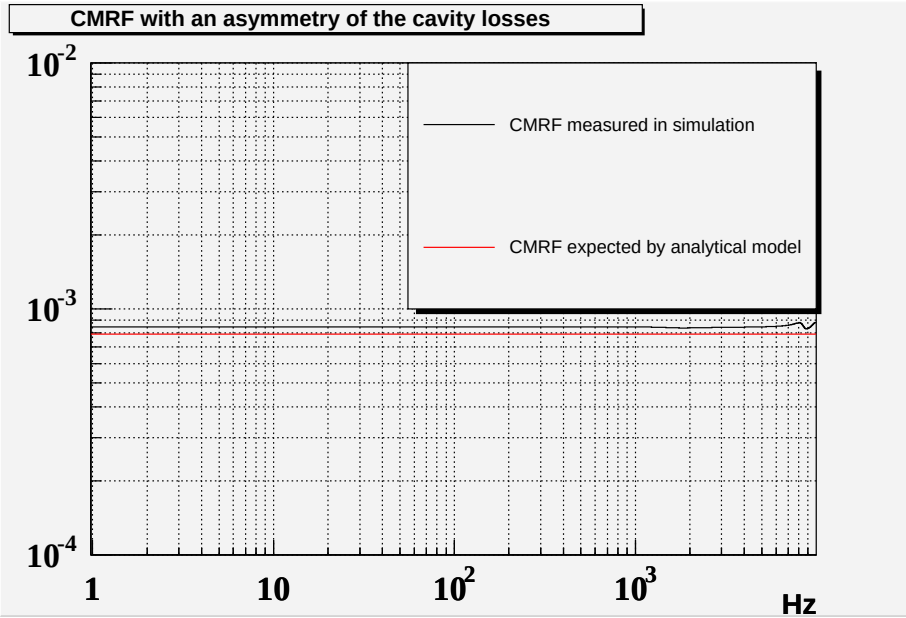

Figure 7: *CMRF due to an asymmetry of the cavity losses.*

losses of 100 ppm, a value of the same order of magnitude than the one expected for the Virgo cavities. The result is shown in Figure 7. The analytical model is in agreement with the simulation within 7%. The values of the optical parameters chosen for this simulation are listed in Table 3. The cavity losses asymmetry has been induced by an asymmetry of the input mirror losses (P_1), while the end mirror losses are put to zero. It has to be noticed that an asymmetry of the end mirror losses would also generate an asymmetry of the Fabry Perot reflectivity modulus but in this case also the finesse would be affected.

Cavity	r_1	r_2	P_1	ρ_{FP}	CMRF
North	0.9389	0.999976	0.4×10^{-3}	0.9936	0.8×10^{-3}
West	0.9389	0.999976	0.3×10^{-3}	0.9952	

Table 3: *Values used in the simulation of an asymmetry between the cavity losses.*

An asymmetry of the cavity losses is able to generate a CMRF of a bit less than one permille assuming an asymmetry of the Fabry Perot round trip losses of one hundred parts per million.

4 Analysis of the C4 run sensitivity

This section is devoted to the identification of noise sources limiting the C4 run sensitivity. For highest frequencies, these sources are laser frequency noise and electronic noise, presented 4.1 and 4.2, and for the lowest frequencies these are actuator noise and control noises presented in 4.3 and 4.4.

4.1 Dark fringe readout noise

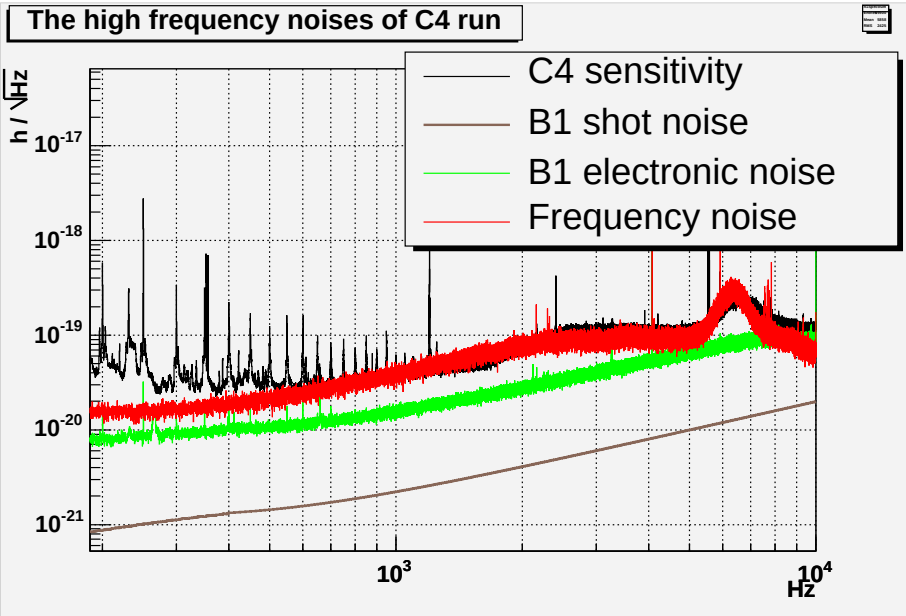

Figure 8: *The high frequency noises of the C4 sensitivity.*

The effect on the sensitivity of the noises identified at high frequency are shown in Figure 8. The electronic noise and the shot noise of the B1 photodiodes which deliver the dark fringe signal have been determined according to the method explained in [5]. The shot noise contribution remains around one order of magnitude below the C4 sentivity and consequently is negligible. As it can be seen in Figure 8 the electronic noise is quite close to the sensitivity but is not the dominant source of noise.

4.2 Laser frequency noise

From 500 Hz to 10 kHz the C4 sensitivity is mainly explained by a laser frequency noise. This noise is introduced by the laser frequency stabilization loop (shown in Figure 1) which uses the $B2\_ACp$ signal as error signal, as explained in section 2. The B2 photodiode electronic noise is propagated to the laser by this loop and then converted into a frequency noise. The B2 shot noise can be neglected because it is lower by about a factor 4 than the electronic noise.

The laser frequency stabilization loop is schematised in Figure 9: n_{elec} refers to the electronic noise entering the error signal and S_p is the signal induced at the B2 photodiode level by a common mode noise. The transfer function between the error signal and the laser frequency noise introduced by the loop is called G_{laser}. The laser frequency noise $\delta\nu$ is equivalent to a common mode fluctuation of the Fabry-Perot cavity length $\delta L = \delta\nu\frac{L}{\nu}$. The sensitivity of the $B2\_ACp$ signal to a δL is characterized by the optical transfer function O_{B2p}. According to this control scheme the laser frequency noise induced by the

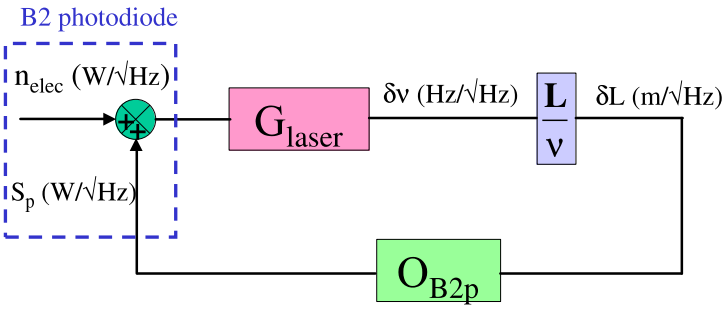

Figure 9: *Laser frequency stabilization loop scheme.*

B2 electronic noise is given by:

$$\delta\tilde{\nu} \;=\; \frac{G_{laser}\,\frac{L}{\nu}}{1 \;-\; H_{laser}}\tilde{n_{elec}} \tag{30}$$

with $H_{laser} = G_{laser}\frac{L}{\nu}O_{B2p}$. H_{laser} is the open loop transfer function which has a high unity gain frequency (typically around 10 kHz). Assuming an infinite gain for H_{laser} the relation (30) can be approximated by:

$$\delta\tilde{\nu} \;=\; \frac{\nu}{L}\frac{1}{O_{B2p}}\tilde{n_{elec}} \tag{31}$$

Then the analytical model giving the contribution of frequency noise in the sensitivity (h) can be written as:

$$h \;=\; \frac{||\delta\tilde{l}||}{L} \;=\; \frac{CMRF}{L}\left|\left|\frac{1}{O_{B2p}}\tilde{n}_{elec}\right|\right| \tag{32}$$

The estimation of laser frequency noise reported in Figure 8 has been computed using this simplified model. Even if the validity of the approximation made to obtain equation (31) is not guaranted for high frequencies, the model explains quite well the sensitivity curve up to 10 kHz, taking into account the fact that the B1 electronic noise also contributes in this region. The B2 electronic noise n_{elec} has been measured when no ligth was reaching the photodiode. The unusual complex shape of the B2 electronic noise spectrum (which is responsible for the bump visible in Figure 8 between 5 kHz and 8 kHz) was due to a cross-talk between some electrical cables. This problem has been solved in December 2005. The parameters CMRF and O_{B2p} of relation (32) are defined as follows:

- The optical response of the B2 photodiode to a common mode noise δL is given by:

$$O_{B2p} \;=\; \frac{K_{B2p}}{1 \;+\; i\frac{f}{f_{cav}}} \tag{33}$$

with $f_{cav} = 500\ Hz$ (according to the Virgo design) and $K_{B2p} = 4.10^3\ W/m$. K_{B2p} is the optical gain of the $B2\_ACp$ signal. It has been obtained experimentally in the recombined configuration by injecting a line at 323 Hz in the correction signals sent to the end mirrors and then measuring the corresponding amplitude in the B2 signal.

- The value of the CMRF has been chosen in order to adjust the model to the sensitivity curve, which gave a constant CMRF equal to 0.003. This value is compatible with a measurement of the CMRF performed during the C4 run by injecting a line at 2432 Hz in the laser frequency stabilization loop and then measuring the corresponding amplitude in the dark fringe signal. This measurement has provided a CMRF ranging between 0.003 and 0.005.

According to the CMRF study performed in section 3, a constant value of the CMRF in the high frequency region is possible if it is limited by an asymmetry of the reflectivity modulus between the two cavities. The CMRF value of 0.003 is compatible with the asymmetry between the two end mirror radii of curvature and a beam mismatching of 5% (see the Table 2). It was also observed that the CMRF is worsened when the alignment conditions are not good. This can be explained since a misalignment of the Fabry Perot cavity mirrors increases the mismatching between the incident beam and the beam resonating inside the cavity. Alternatively such a CMRF could be explained by a difference of 300 parts per million between the round trip losses in the two Fabry Perot cavities. Such an asymmetry of losses seems a little bit too large: a simulation study presented in [6], which uses the maps of the mirror substrates and the maps of the mirror coatings, gives an asymmetry of losses of about 60 ppm. Nevertheless the measurement of the cavity losses and of the recycling gain made so far are not precise enough to exclude an asymmetry of 300 ppm.

4.3 Actuator noise

The actuator noise refers to the electronic noise generated by the Digital Analog Convertors (DAC) and the coil drivers used to act on the mirror position. This noise produces a mirror displacement δL_{mirror} which is likely to limit the sensitivity. A simplified scheme of the mirror actuation chain is presented in Figure 10. The actuator noise is estimated by reading the current δi passing through the coil when no correction signal is sent to the DAC. Then this current can be converted into an equivalent voltage δu at the DAC output level, knowing the coil driver gain and the coil parameters (resistor and inductance). An example of measurement performed in the north input tower during the C4 run is shown in Figure 11. The noise is expressed at the DAC output level ($V/\sqrt{Hz}$).

The mirror position noise δL_{mirror} induced by the actuator noise δu for one coil is given by:

$$\delta L_{mirror} \ = \ ||K_{DC}\ E\ M\ \delta\tilde{u}|| \tag{34}$$

where:

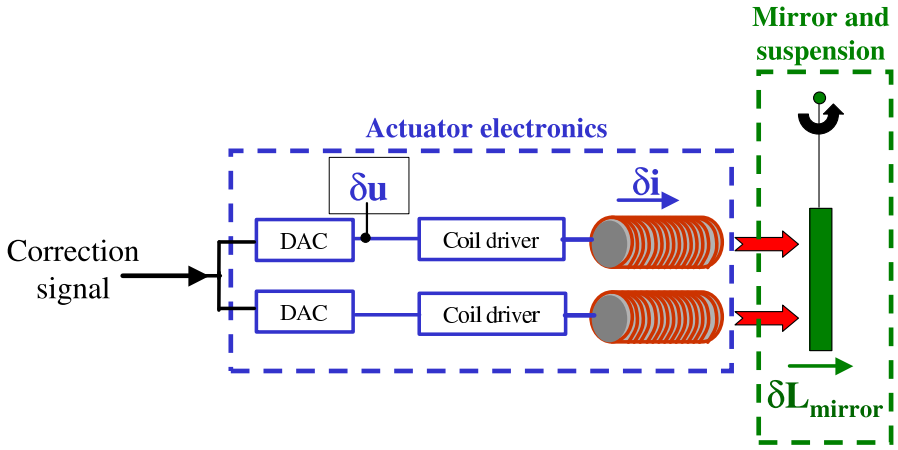

Figure 10: *Scheme of the mirror actuator chain.*

- K_{DC} is the mirror displacement produced when one Volt is applied to the DAC. The calibration measurements described in [7] give an actuation gain $K^{\star}_{DC,z} \approx 12\ \mu m/V$ between the correction signal and the mirror displacement for the arm towers. There is an uncertainty of 20% on this measurement. As two coils are used to control each mirror, one obtains: $K_{DC} = \frac{K^{\star}_{DC,z}}{2} \approx 6\ \mu m/V$. It is different for the beam splitter mirror which is about four times lighter than the other mirrors. The value measured with C4 data is: $K_{DC} \approx 34 \pm 7\ \mu m/V$. This value has been obtained during the run from a measurement of the amplitudes of the permanent calibration lines on the NE (at 353 Hz), the WE (at 355 Hz) and BS (at 357 Hz). It makes use of the knowledge of the value of K_{DC} for the NE and the WE mirrors as well as the coils cut-off frequency. The uncertainty on these values leads to a precision on K_{DC} of 20%.

- E is the electrical response of the coil which can be written as:

$$E = \frac{1}{1 + i\frac{f}{f_{coil}}} \tag{35}$$

  With $f_{coil} = \frac{R_{coil}}{L_{coil}}$ and R_{coil} and L_{coil} are the coil resistor and inductance. According to the C4 design this frequency was around 480 Hz. The calibration measurements in [7] rather give values around 800 Hz and 900 Hz for the north end and the west

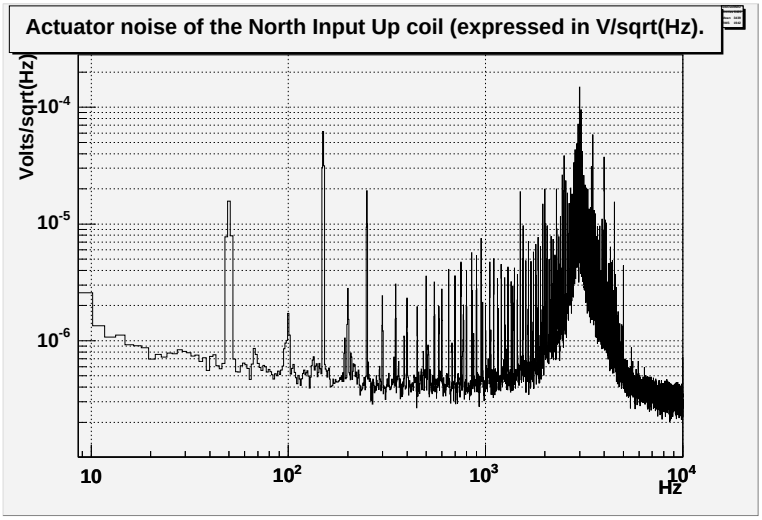

Figure 11: *Example of an actuator noise measurement performed during C4.*

end towers respectively but it was not taken into account for the actuator noise estimation. In any case E can be approximated to 1 in the frequency region where the sensitivity is dominated by actuator noise.

- M is the mechanical response of the mirror wich behaves as a pendulum resonating at $f_{mirror} = 0.6\ Hz$:

$$M = \frac{1}{1 + i\frac{1}{Q}\frac{f}{f_{mirror}} - \left(\frac{f}{f_{mirror}}\right)^2} \tag{36}$$

The effect of the quality factor Q can be neglected in the Virgo bandwidth.

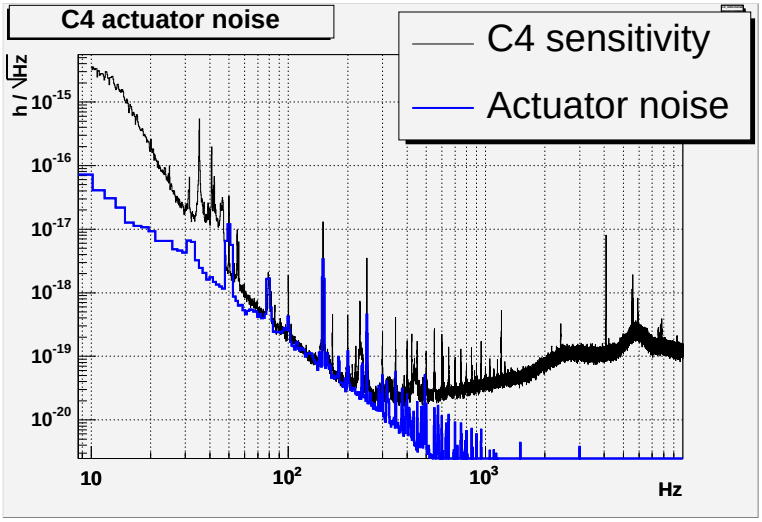

Figure 12: *The actuator noise during the C4 run.*

For what concerns the four arm mirrors, the longitudinal displacement due to actuator noise produces a differential length variation of the Fabry Perot cavity which is directly

equivalent to the effect of a gravitationnal wave, so that one can write: $\delta l = \delta L_{mirror}$, where δl refers to the noise contribution in the sensitivity. During the C4 run two coils were used for each of the four cavity mirrors. The total contribution in sensitivity of the arm mirror actuator noise is obtained by adding quadratically the contribution of each of these eigth coils. The estimation of the C4 actuator noise is compared to the sensitivity curve in Figure 12: It limits the sensitivity between 70 and 300 Hz. This estimation has been obtained from a measurement performed on both north and west input towers, assuming that the noise of the end mirror actuators were at the same level. The measurement gave an averaged actuator noise equivalent to a DAC output voltage of 880 $nV/\sqrt{Hz}$ for each coil.

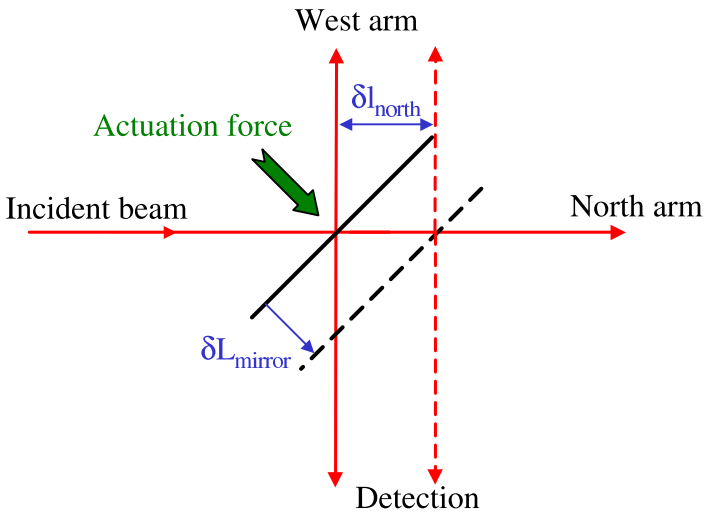

Figure 13: *Arm length variation created by a longitudinal motion of the beam splitter.*

A variation of the longitudinal position of the beam splitter mirror is also likely to affect the sensitivity because it produces a length asymmetry between the two arms. As it is shown in Figure 13 the beam splitter motion δL_{mirror} induced by the actuator keeps the length of the west arm unchanged whereas the length of the north arm varies by a quantity δl_{north} given by:

$$\delta l_{north} = \sqrt{2}\, \delta L_{mirror} \tag{37}$$

Nevertheless a length variation of the short Michelson arm has less impact in the sensitivity than a length variation of the Fabry Perot cavity in which the resonant beam makes several round-trips. Therefore the contribution in sensitivity of the beam splitter longitudinal noise is reduced by a factor $\frac{2F}{\pi} = 32$ which is the number of round-trips. Finally the contribution in sensitivity of a beam splitter motion δL_{mirror} can be written as:

$$h \;=\; \frac{\delta l}{L} \;=\; \frac{\sqrt{2}}{L}\,\frac{\pi}{2F}\,\delta L_{mirror} \;=\; \frac{1}{22.6}\,\frac{\delta L_{mirror}}{L} \tag{38}$$

According to relation (38) and considering that the beam splitter mirror is four times lighter, the impact in sensitivity of the actuation noise of one single coil is expected to be about 4 times lower for the beam splitter than for the other mirrors. Consequently taking into account that four coils instead of two are plugged in the beam splitter tower, the impact in sensitivity of the actuator noise generated in this tower is about a factor 3 lower than the impact of one single arm tower. The conclusion is that the beam splitter actuator noise of the C4 run can be neglected.

4.4 Beam splitter control noises

The lowest frequency region of the C4 sensitivity (below 60 Hz) is mainly limited by noise injected via the longitudinal and angular control of the beam splitter (BS) mirror. In this section it is first explained how the BS control noises have been identified and how their contribution in sensitivity has been estimated. Then the analytical models describing the propagation of these noises into the dark fringe are presented. Finally a further analysis which has been performed in order to understand the origin of the noise in the error signal of the BS longitudinal control loop is presented.

4.4.1 Contribution of the BS control noises in sensitivity

The largest coherences between the dark fringe signal and the interferometer control signals are shown in Figure 14 and have been found to be:

- the locking correction signal sent to the beam splitter actuators for the control of its longitudinal position (top left plot);
- the angular correction signal sent to the beam splitter actuators to control the θ_x degree of freedom, i.e. the rotation around the horizontal axis (top right plot);
- the θ_x angular correction signals applied to the marionette for both west input and west end mirrors (bottom left and bottom right plots respectively).

Some lower coherence has also be found between the dark fringe signal and the θ_y angular correction signals applied to the marionette of the four arm mirrors (θ_y refers to the rotation around the vertical axis of the mirror).

One can notice in Figure 14 that the dark fringe signal has a large coherence with all the four control signals between 10 and 30 Hz, so that it is not possible to identify directly the control loop which is effectively responsible for the noise limiting the sensitivity in this region. Moreover these four control signals are coherent between each other which means that the corresponding degrees of freedom are coupled. In fact the west arm mirrors are expected to follow the beam splitter motion due to the linear alignment, while the beam splitter is only under local control. This can explain the coherence observed between

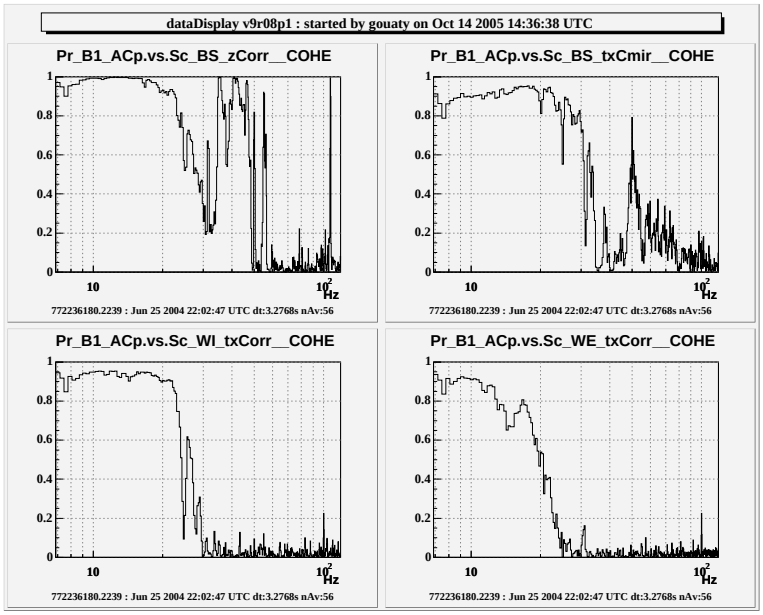

Figure 14: *Some coherence functions measured with C4 data between the dark fringe signal and several control signals in the 10-100 Hz region.*

the west arm angular corrections and the dark fringe signal if the noise is introduced at the beam splitter level. Consequently in the following we will assume that the noise is introduced by the beam splitter angular and longitudinal control.

The coherence between these two correction signals, shown in Figure 15, again indicates a coupling between the θ_x and the longitudinal motion of the mirror. A more sophisticated computation, called cross-coherence computation, has been performed in order to better identify the contribution of each of these two correction signals in the sensitivity. This computation is explained in the following.

The amplitude spectrum of the noise entering the dark fringe signal (denoted as X_0) is assumed to be composed of three contributions:

$$X_0 \;=\; aX_1 + bX_2 + cX_3 \tag{39}$$

where X_1 refers to the beam splitter longitudinal correction signal, X_2 to the beam splitter θ_x angular correction signal, and X_3 is the possible remaining noise which is supposed to be incoherent with the two previous signals. X_0, X_1, X_2, and X_3 are normalised by their amplitude spectrum modulus so that the coherence function can be defined as a scalar product between these elements. The complex transfer functions a, b and c can be computed by solving a linear system:

$$\left\{ \begin{array}{l} < X_1, X_0 > = a < X_1, X_1 > \; + b < X_1, X_2 > \; + c < X_1, X_3 > \\ < X_2, X_0 > = a < X_2, X_1 > \; + b < X_2, X_2 > \; + c < X_2, X_3 > \\ < X_3, X_0 > = a < X_3, X_1 > \; + b < X_3, X_2 > \; + c < X_3, X_3 > \end{array} \right. \tag{40}$$

which simplifies into:

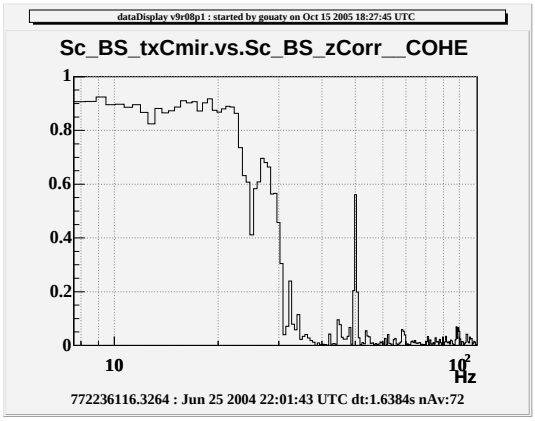

Figure 15: *Coherence function between the longitudinal correction and the θ_x angular correction applied to the beam splitter mirror.*

$$\begin{cases} < X_1, X_0 > = a \ + \ b < X_1, X_2 > \\ < X_2, X_0 > = \ a < X_2, X_1 > + b \\ < X_3, X_0 > = \qquad\qquad c \end{cases} \tag{41}$$

The notation $< X, Y >$ refers to the complex coherence between the variables X and Y. The quantities a and b are deduced from the measurement of these coherence functions. The total contribution of beam splitter control noises in the dark fringe signal given by:

$$\delta n_{BS} \ = \ B1\_ACp \ \sqrt{||a||^2 + ||b||^2 + 2Re(\bar{a}b < X_1, X_2 >)} \tag{42}$$

where $B1\_ACp$ refers to the amplitude spectrum of the dark fringe signal. In this equation the term $2Re(\bar{a}b < X_1, X_2 >)$ takes into account the coupling between z and θ_x degrees of freedom. In a general case this term can be positive or negative according to the interference between the two noise sources. In the example of the C4 run data the corrective term has a positive sign so that it makes sense to define a common contribution of BS control noises (denoted as $n_{BS,common}$), and single contributions of both BS longitudinal and angular control noises (respectively denoted as $n_{BS,z}$ and $n_{BS,tx}$) by these relations:

$$\delta n_{BS,z} \ = \ B1\_ACp \ ||a|| \tag{43}$$

$$\delta n_{BS,tx} \ = \ B1\_ACp \ ||b|| \tag{44}$$

$$\delta n_{BS,common} \ = \ B1\_ACp \ \sqrt{2Re(\bar{a}b < X_1, X_2 >)} \tag{45}$$

The noise contributions in sensitivity are obtained by multiplying $\delta n_{BS,z}$, $\delta n_{BS,tx}$ and $\delta n_{BS,common}$ (expressed in $W/\sqrt{Hz}$) by the calibration transfer function. The results are

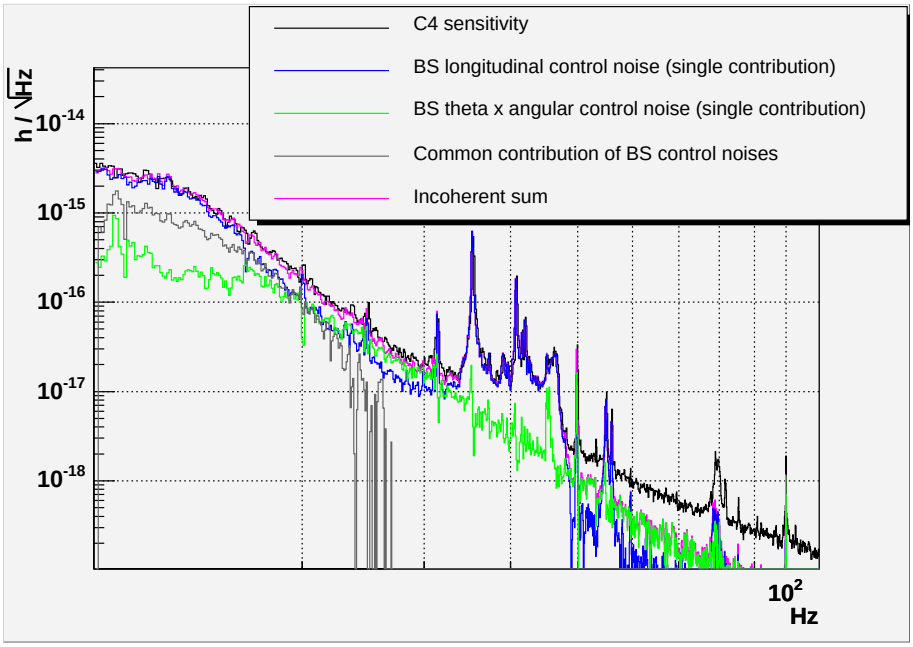

Figure 16: *Contribution of the beam splitter (BS) control noises in the C4 sensitivity. These estimations have been obtained with the cross-coherence computation.*

presented in Figure 16. The curve called "incoherent sum" gives the estimate of the total beam splitter control noises as given by relation (42). According to this evaluation the beam splitter control noises explains the C4 sensitivity at least between 10 and 50 Hz. The beam splitter longitudinal control noise limits the sensitivity between 10 and 16 Hz and in the 30-56 Hz region where quite complex structures are visible. The beam splitter θ_x angular control noise is domimant between 24 and 30 Hz. Between 16 and 24 Hz all thse noise sources contribute at the same level.

4.4.2 Analytical models for the propagation of BS control noises

The coherence computation has helped to identify the noise sources but the propagation mechanisms have still to be understood. Analytical models to propagate the angular and longitudinal control noises are proposed hereafter.

Angular control noise

The coupling mechanism between the beam splitter θ_x angular control noise and the dark fringe signal could be explained by two simple hypothesis.

The first one consists in assuming that the beam splitter mirror actuators are not symmetrical. Then an angular correction signal induces both angular and longitudinal motions of the mirror. The longitudinal displacement of the beam splitter affects the sensitivity according to relation (38). Nevertheless the actuator asymmetry required to explain the coupling observed during the C4 run is about 40% which does not seem realistic.

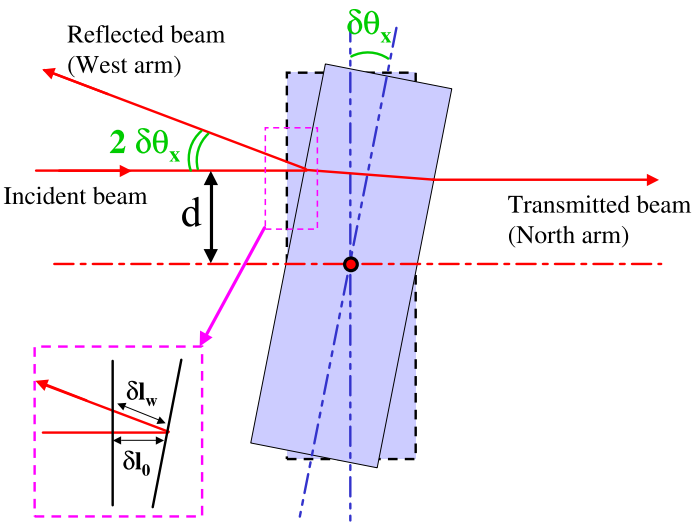

Figure 17: *Effect of a θ_x angular motion of the beam splitter (in profile view).*

The second hypothesis assumes that the incident beam is vertically miscentered with respect to the beam splitter mirror. The situation is schematized in Figure 17. d is the vertical miscentering of the beam and $\delta\theta_x$ refers to the angular motion of the mirror due to the control noise. As can be seen in Figure 17 the beam splitter angular motion induces a variation

$$\delta l_w \approx \delta l_0 = d\ \delta\theta \tag{46}$$

The beam transmitted to the north arm sees a variation δl_n of its optical path such as: $\delta l_n = -\delta l_w$. As a consequence the beam splitter angular control noise generates an asymmetry δl_{mich} of the short Michelson arms given by:

$$\delta l_{mich} \approx 2\ d\ \delta\theta \tag{47}$$

The noise contribution in sensitivity is obtained by subtituting $\sqrt{2}\ \delta l_{mirror}$ by δl_{mich} in relation (38). The beam splitter θ_x angular motion is deduced from the correction signal BStxCmir using the relation:

$$\delta\tilde{\theta} = ||K^{\star}_{DC,\theta_x}\ E\ M_{\theta_x}\ \tilde{BStxCmir}|| \tag{48}$$

where $K^{\star}_{DC,\theta_x} \approx 45\mu rad/V$ is the angular actuation gain between the correction signal and the effective mirror rotation. The actuator electrical transfer function E is the same as in (35), and the mechanical response M_{θ_x} is given by a second order low pass filter with a double pole at 3.3 Hz. The contribution in sensitivity of the beam splitter angular control noise can be finally written as:

$$h = \frac{\delta l}{L} = \left|\left|\frac{2\ d}{L}\ \frac{\pi}{2F}\ K^{\star}_{DC,\theta_x}\ E\ M_{\theta_x}\ \tilde{BStxCmir}\right|\right| \tag{49}$$

The previous analytical model has been adjusted to the measured sensitivity by assuming $d = 1.55\ cm$, which is a large but realistic miscentering. As shown in Figure 18, this

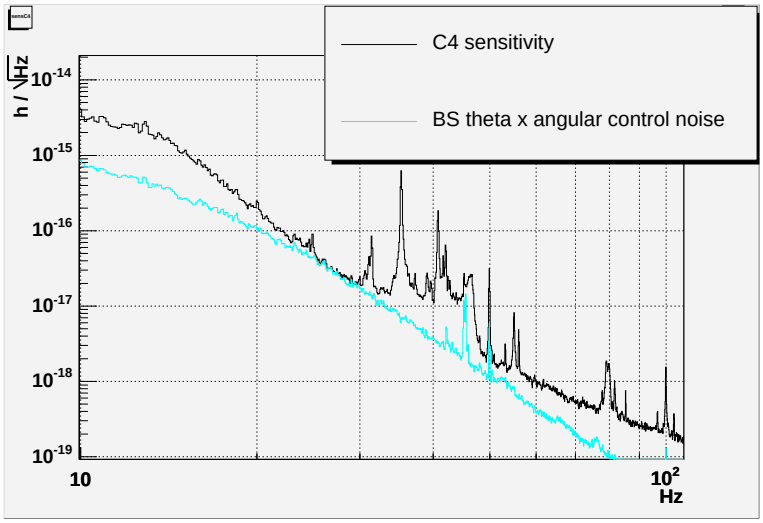

Figure 18: *Beam splitter θ_x angular control noise estimated with the analytical model, assuming a miscentering of 1.55 cm.*

model fits well to the sensitivity curve between 24 and 30 Hz and also partially explains the sensitivity around 50 Hz.

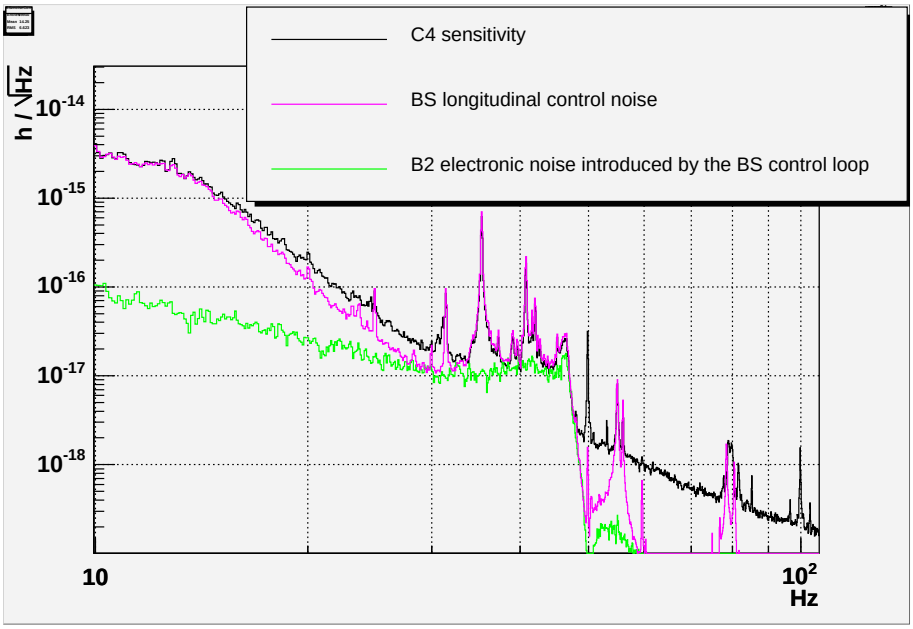

Figure 19: *Beam splitter longitudinal control noise estimated with the analytical model.*

Longitudinal control noise

The beam splitter longitudinal correction signal is responsible for a mirror displacement δL_{mirror} which can be deduced from relation (34), taking into account the fact that the locking force on the beam splitter mirror is generated by four coils and that the

correction signal $BSzCorr$ is divided by two before being sent to the DAC:

$$\delta L_{mirror} \;=\; ||2\; K_{DC}\; E\; M\; BS\tilde{zCorr}|| \tag{50}$$

The analytical model giving the contribution of beam splitter longitudinal control noise in the sensitivity is obtained by combining relations (50) and (38):

$$h \;=\; \frac{\delta l}{L} \;=\; \left|\left|\frac{\sqrt{2}}{L}\;\frac{\pi}{2F}\;2\;K_{DC}\;E\;M\;BS\tilde{zCorr}\right|\right| \tag{51}$$

The noise projection provided by this model is shown in Figure 19. The DC conversion factor from DAC output voltage to longitudinal mirror displacement (K_{DC}) has been measured for C4, $K_{DC} = 34\ \mu m/V$, with an uncertainty of 20%. The estimation of the beam splitter longitudinal control noise gives similar structures as the ones observed in the 30-56 Hz region in the sensitivity curve with similar amplitude. The model also explains quite well the 10-16 Hz region of the sensitivity curve.

The results obtained with the analytical models used to propagate both BS longitudinal and angular control noises confirm the prediction made with the cross-coherence computation (shown in Figure 16). The beam splitter control loops have been identified as being responsible for the propagation of noise into the interferometer output port. The noise visible in the BS angular correction signal most likely comes from the readout noise of the local control sensors. The noise introduced by the BS longitudinal control loop cannot be explained so easily. It can be helpful for noise reduction purpose to understand what the origin of that noise is and how it couples to the error signal of this control loop.

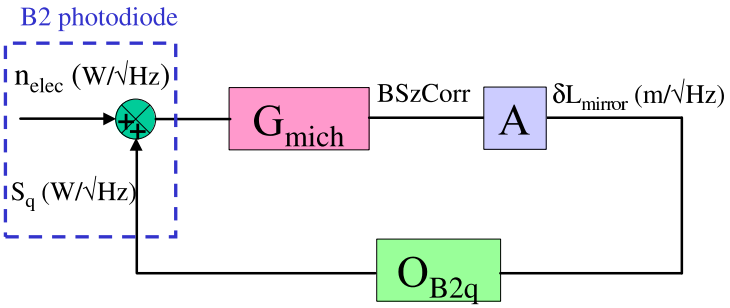

Figure 20: *Scheme of the beam splitter longitudinal control loop.*

4.4.3 Origin of the noise in the BS longitudinal control loop

The error signal of the BS longitudinal control loop is provided by the $B2\_ACq$ signal, as explained in section 2. First the electronic noise of B2 photodiode was suspected. A

scheme of the beam splitter longitudinal control loop is presented in Figure 20. G_{mich} is the transfer function of the filter implemented between the error signal and the correction signal, O_{B2q} is the optical response of the $B2\_ACq$ signal to a beam splitter mirror displacement, and A is the global actuator transfer funtion: $A = 2\ K_{DC}\ E\ M$. The contribution in sensitivity of the B2 electronic noise is given by:

$$h = \frac{\delta l}{L} = \left\| \frac{\sqrt{2}}{L} \frac{\pi}{2F} \frac{A\ G_{mich}}{1 - H_{mich}} \tilde{n}_{elec} \right\| \tag{52}$$

where $H_{mich} = A\ G_{mich}\ O_{B2q}$ is the open loop transfer function of the beam splitter longitudinal control. For frequencies higher than unity gain (which is typically around 10 Hz) the relation (52) can be approximated by:

$$h \approx \left\| \frac{\sqrt{2}}{L} \frac{\pi}{2F} A\ G_{mich}\ \tilde{n}_{elec} \right\| \tag{53}$$

The modulus of the transfer function G_{mich} is presented in Figure 21. The scheme shown in Figure 20 is relevant only if the coupling with the other locking control loops is negligible. A Siesta simulation has been performed in order to check that no significant effect was visible due to the other locking control loops. The photodiode electronic noises were also included. The simulation has confirmed the validity of the analytical model given by (53). This model has been used to obtain the estimation of the impact in the sensitivity of the B2 electronic noise which is shown in Figure 19. It can be concluded than the B2 electronic noise cannot explain the beam splitter longitudinal control noise observed during the C4 run. Another possible origin of the noise has to be found.

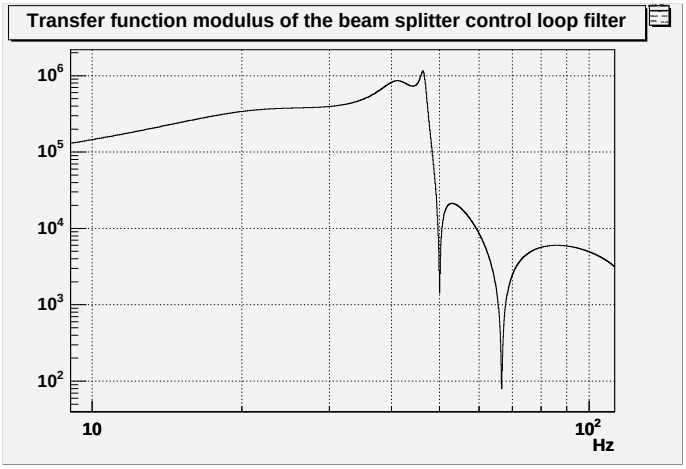

Figure 21: *Modulus of the transfer function of the filter implemented in the beam splitter longitudinal control loop.*

In fact, most of the structures visible in the sensitivity curve between 30 and 60 Hz and explained by the beam splitter longitudinal control noise model have been identified as input bench mechanical resonances [8]. A measurement of these resonances has been performed on February 2005: It has been obtained by computing the transfer function

between a noise injected into the input bench coils, to produce a longitudinal motion, and the reference cavity error signal which is sensitive to input mode cleaner length fluctuations. The result of the measurement is shown in arbitrary units in Figure 22, where it is compared to the spectrum of the *B2_ACq* signal obtained during the C4 run. Most of the peaks present in the error signal of the beam splitter longitudinal control loop can be associated to the input bench mechanical resonances. It must be noted that the frequency of these resonances can drift when the bench is too much shaken, which explains why some of the resonances visible in Figure 22 are not exactly at the same frequency for both curves. The coupling mechanism is explained in the following.

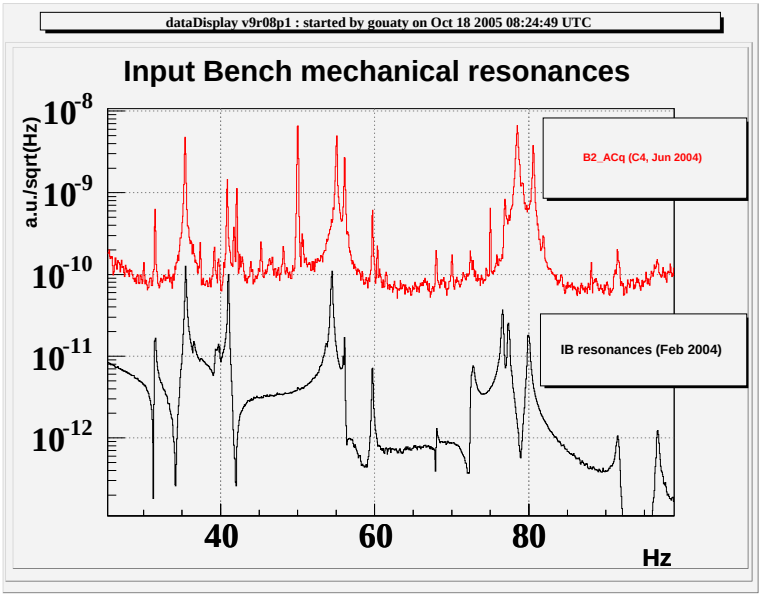

Figure 22: *Comparison between a measurement of the input bench (IB) resonances performed on Febrary 2004 and the B2_ACq spectrum observed during the C4 run (June 2004).*

The input bench resonances in the 30-60 Hz region correspond to two kinds of mechanical effects:

- the violin modes of the suspension wires;
- the modes of the system formed by the bench, marionette and wires which induces vertical translation and angular motion around the two horizontal axis of the input bench.

These resonance modes are suspected to be excited by the input bench local control and actuator noises. Then they generate input mode cleaner length fluctuations which modifies the conditions of resonance of the beam.

The input mode cleaner cavity length and the laser frequency are controlled in order to satisfy the resonance condition for the carrier. In ideal conditions the modulation frequency ν_{mod} should be tuned so that the two side-bands are also resonant in the mode

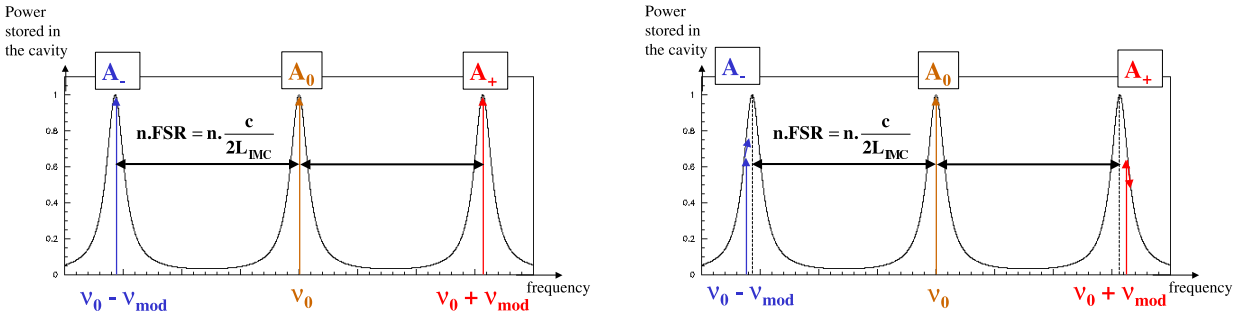

Figure 23: *Power stored in the input mode cleaner cavity as a function of the frequency. The modulation frequency is correctly tuned in the left plot, while it is detuned in the right plot. The maxima that should be found between each side-band and the carrier are not represented for clarity reasons.*

cleaner cavity. This situation is schematized in the left plot of Figure 23. The curve represents the power in the cavity as a function of the frequency of the laser component, in arbitrary units. The vertical arrows indicate the spectral position of the two side-bands and the carrier. All are located at a resonant point:

$$\nu_0 \; = \; qFSR \qquad \nu_0 \pm \nu_{mod} \; = \; (q \pm n)FSR \quad (with \; q \; >> \; n) \tag{54}$$

The FSR (free spectral range) is the spectral distance between two maxima of the power: $FSR \; = \; \frac{c}{2L_{IMC}}$, where L_{IMC} is the mode cleaner cavity length. The effect of a mode cleaner length variation is equivalent to a drift of the frequency axis in Figure 23. If the modulation frequency is correctly tuned to the FSR, a mode cleaner length noise does not modify the amplitude of the side bands in the first order approximation. In this case it is just equivalent to a laser frequency noise which should not be seen by the $B2\_ACq$ signal.

On the contrary, if the modulation frequency is mistuned, the two side-bands are no more perfectly resonant in the input mode cleaner cavity. This situation is illustrated by the right plot of Figure 23. In this case a mode cleaner length fluctuation generates a first order variation of the two side-band amplitudes. For example, for a too large modulation frequency, if the mode cleaner length increases, the amplitude of the left side-band increases whereas the amplitude of the right side-band decreases. The field reaching the B2 photodiode can be written as:

$$E \; (t) = \; A_0^{B2} e^{i2\pi\nu_0 t} \; + \; A_+^{B2} e^{i2\pi(\nu_0+\nu_{mod})t} \; + \; A_-^{B2} e^{i2\pi(\nu_0-\nu_{mod})t} \tag{55}$$

With: $A_0^{B2} \; = \; P_0 A_0 \; , \quad A_+^{B2} \; = \; P_+ A_+ \; , \quad A_-^{B2} \; = \; P_- A_-$
P_0, P_+ and P_- are the operators which describe the field propagation inside the interferometer. The two arms are assumed to be symmetrical so that it is not needed to take into account the effect of the interference at the beam splitter level. The amplitude variation of the side-bands is described thanks to the field propagation operators by writting:

$$P_0 \; = \; a \; e^{i\phi} \; ; \qquad P_+ \; = \; b(1+\epsilon) \; e^{i\phi} \; ; \qquad P_- \; = \; b(1-\epsilon) \; e^{i\phi} \tag{56}$$

The phases of the carrier and the two side-bands are assumed to vary in a similar way ; a, b and ϵ are real numbers. The in-phase demodulated signal S_p and the in-quadrature demodulated signal S_q are given by:

$$S_p \ = \ -Im(A_+\bar{A}_0 \ + \ A_0\bar{A}_-) \tag{57}$$

$$S_q \ = \ Re(A_+\bar{A}_0 \ + \ A_0\bar{A}_-) \tag{58}$$

which finally gives:

$$S_p \ = \ 0 \quad and \quad S_q \ = \ 2abA^2J_1(m)J_0(m)\epsilon \tag{59}$$

This result shows that a mistuning of the modulation frequency with respect to the input mode cleaner length makes the in-quadrature B2 signal ($B2\_ACq$) sensitive to a mode cleaner length noise. This mechanism explains how the input bench mechanical resonances couple to the error signal of the beam splitter longitudinal control loop. The required mistuning for the modulation frequency during the C4 run has been estimated to be around 70 Hz. This corresponds to the value found when the modulation frequency was retuned.

Finally the origin of the noise introduced by the beam splitter longitudinal control loop above 30 Hz is well understood, whereas the noise injected by this loop between 10 and 30 Hz has not been clearly identified: since there is a large coherence with the beam splitter angular control noise (as shown in Figure 15) it can be explained as a coupling of angular and longitudinal control noises.

4.5 Noise budget of the C4 run

The main results of the analysis of the C4 run sensitivity are summarized in Figure 24 where all the contributions of the identified noise sources are shown. The C4 run sensitivity has been well understood except for what concerns some structures in the 200-700 Hz region. From 10 to about 300 Hz the sensitivity is limited by two kinds of control noise: the beam splitter longitudinal and angular control noises (which refer to some noise visible in the correction signals), and the mirror actuator noise. At higher frequencies the sensitivity is limited by the laser frequency noise induced by the electronic noise of the error signal $B2\_ACp$. However it must be noticed that the electronic noise of the dark fringe signal is quite close to the sensitivity at high frequency. The upgrades which arose from this analysis are discussed in the next section.

5 Analysis of the C5 run sensitivity

The results of the analysis of the C5 run sensitivity are presented in this section. The technical improvements which have allowed some noise reduction with respect to the C4 run sensitivity are emphasized.

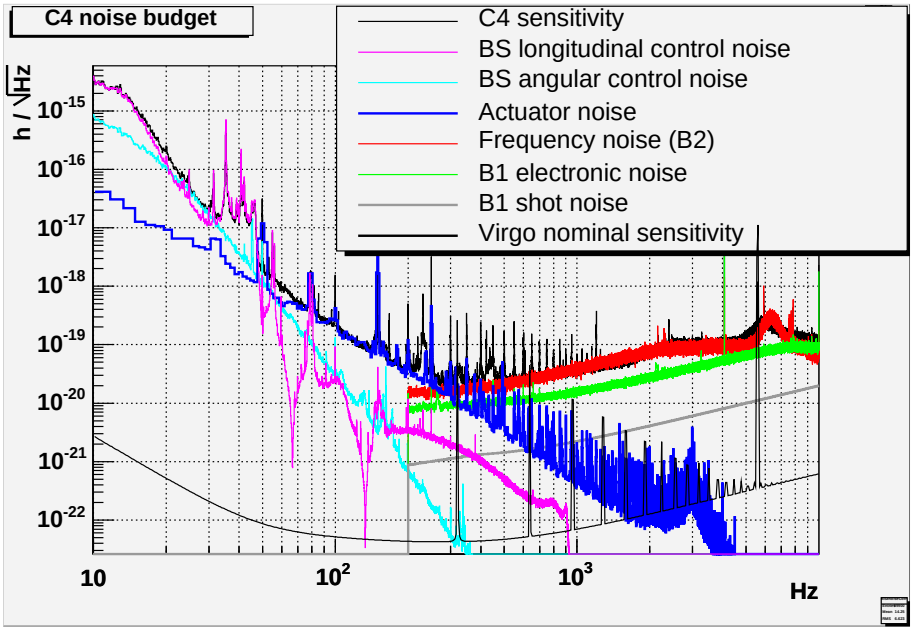

Figure 24: *Noise budget of the C4 run.*

5.1 Dark fringe readout and laser frequency noise

The high frequency noise contributions in the C5 sensitivity are shown in Figure 25. The situation has changed with respect to the high frequency noises of the C4 sensitivity (Figure 8). This is due to the change in the optical setup of the injection bench which has been mentionned in section 2. The consequences for the sensitivity of this optical modification are the following:

- The power entering the interferometer is divided by 10. This produces a drop of the signal to noise ratio of the B1 photodiode. As a consequence the impact in sensitivity of the B1 electronic noise is expected to be increased by a factor 10. Therefore the C5 sensitivity is limited by the B1 electronic noise from 300 Hz to 10 kHz.

- The amount of power reaching the B2 photodiode is increased by a factor 30 so that the contribution of the laser frequency noise due to the B2 electronic noise is expected to be reduced by the same factor. This is the reason why the contribution of the laser frequency noise shown in Figure 25 is much lower than the C5 sensitivity. This estimation is obtained using the same analytical model as the one described in section 4.1, with a CMRF equal to 0.003. This value has been confirmed experimentally during the C5 run by injecting a line at 4511 Hz in the laser frequency stabilisation loop. It can be noted that the CMRF is not constant for lower frequencies. Indeed other measurements performed at 27 and 444 Hz give CMRF values equal respectively to 0.027 and 0.015.

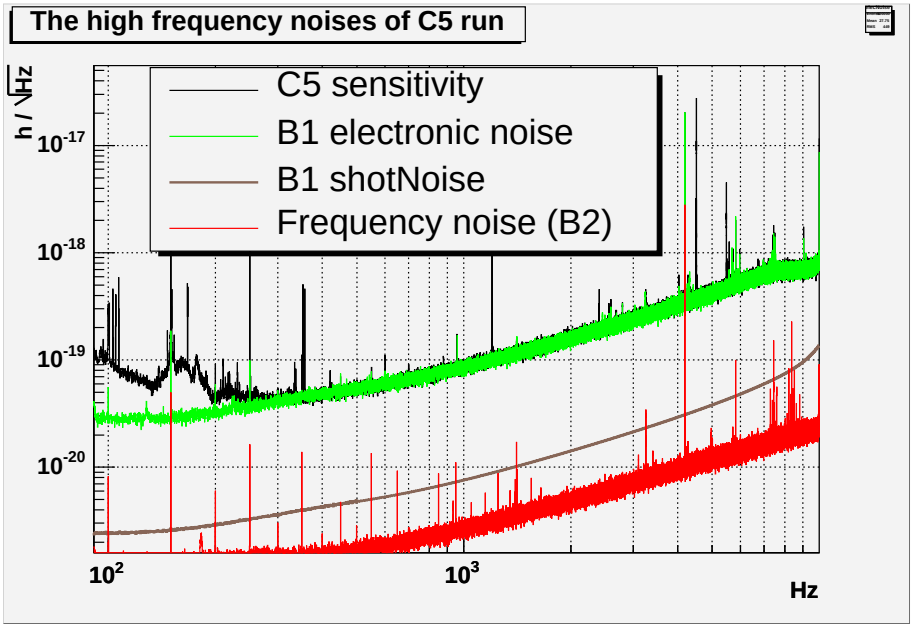

Figure 25: *The high frequency noises of the C5 run.*

5.2 Actuator noise

Since the actuator noise had been identified as a noise limiting the C4 sensitivity, some upgrades were brought to the actuator electronics. The current generated by the DAC and coil driver noise can be reduced adding a serial resistor R_{serie} with the coil. The attenuation factor of the actuator noise k_a is then given by:

$$k_a = \frac{R_{coil}}{R_{coil} + R_{serie}} \tag{60}$$

where R_{coil} refers to the intrinsic resistor of the coil: $R_{coil} \approx 11\ \Omega$. With this method the correction signal has to be multiplied by $\frac{1}{k_a}$ before being sent to the DAC in order to apply the same force on the mirror. As the correction signal cannot exceed the saturation voltage of the DAC, the maximum force that can be applied to the mirror is lowered. Therefore, other technical upgrades are needed in order to reduce the dynamic range of the locking correction signals:

- The actuator electronics are rearranged so that, during the acquisition of the lock, the noisier electronics are used in order to be able to apply large forces on the mirrors, and when the interferometer reaches its working point, the low noise configuration is switched on.

- When the interferometer is fully locked, the hierarchical control strategy makes it possible to reduce the dynamic range of the correction applied to the mirror since the low frequency part of the correction signal is allocated to the marionette. It must be mentionned that the marionette actuator noise does not limit the sensitivity thanks to the mechanical filtering effect between the marionette and the mirror.

During the C5 run a serial resistor of 250 Ω was implemented in the actuation chain of the four arm mirrors, which corresponds to: $k_a = 0.0423$. A measurement of the

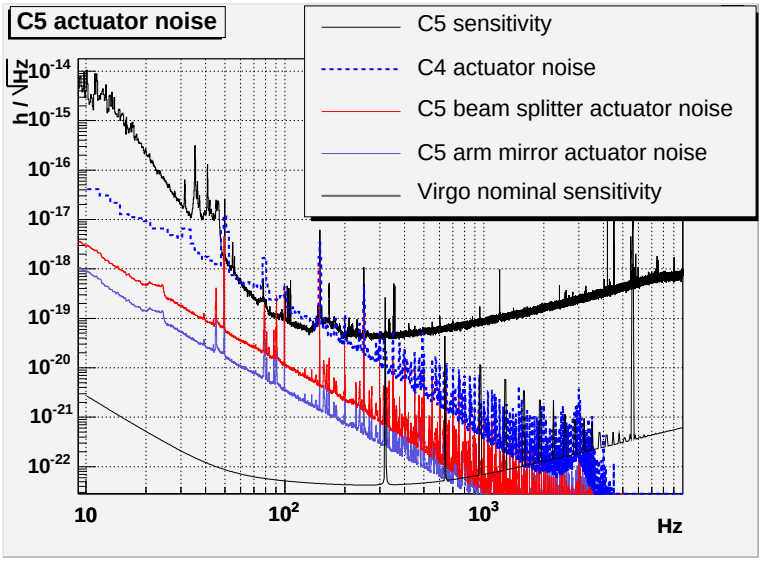

Figure 26: *The actuator noise during the C5 run. The C4 actuator noise has been included for comparison.*

actuator noise in low noise configuration was performed in January 2005 on the coils Up and Down of each arm tower. It gave an averaged actuator noise equivalent to a DAC output voltage $\delta u = 440\ nV/\sqrt{Hz}$ for each coil, which is two times lower than the result of the measurement performed on the input towers during the C4 run. The total contribution in sensitivity of the actuator noise of the arm mirrors is estimated from this new measurement by using the following analytical model deduced from relation (34):

$$h = \frac{\delta l}{L} = ||\sqrt{8}\ k_a\ K_{DC}\ E\ M\ \delta\tilde{u}|| \tag{61}$$

where $\sqrt{8}$ is for the quadratic sum on the eight coils. K_{DC}, E and M are unchanged with respect to the description given in 4.2.1, except for what concerns the pole f_{coil} which is now given by: $f_{coil} = \frac{R_{coil}+R_{serie}}{L_{coil}}$ and the value of K_{DC} for the beam splitter which has been remeasured with C5 data with the same method as described in 4.3: $K_{DC} = 25\mu m/V$ with an uncertainty of about 20%. According to this estimation, the actuator noise due to the arm mirror coils is expected to be reduced by about a factor 50 with respect to the C4 actuator noise. This is shown in Figure 26. The contribution of the beam splitter actuator noise is also included. It is estimated by extrapolating the measurement performed on the arm towers to the beam splitter. Since no upgrade was performed on this tower before the C5 run, the contribution of its actuator noise is now a factor 3 higher than that of the four arm towers.
As it can be seen in Figure 26 the C5 sensitivity should not be limited by the actuator noise which is one order of magnitude lower according to the previous estimation. One must keep in mind that the actuator noise was measured when no correction was sent to the DAC. The analysis of the commissioning runs performed since then has shown that an additional non linear noise can be measured in the coil when a correction signal is applied to the DAC. Consequently the actuator noise shown in Figure 26 could be underestimated.

5.3 Beam splitter control noises

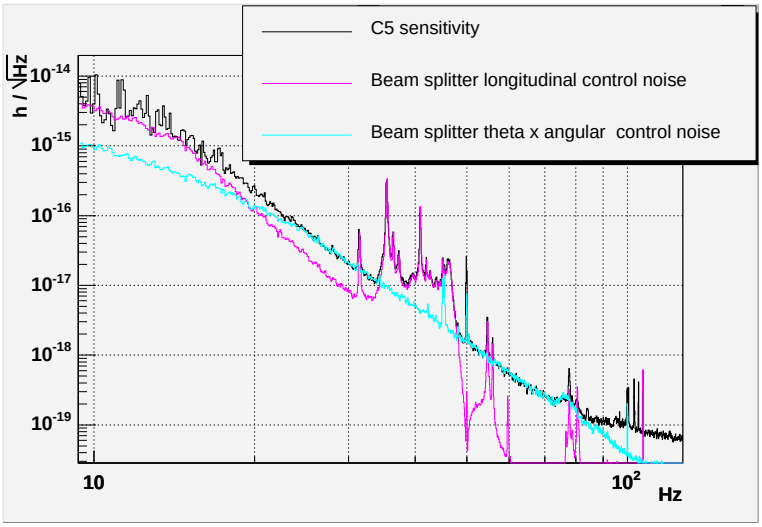

Figure 27: *Contribution of the beam splitter control noises in the C5 sensitivity.*

Below 80 Hz the sensitivity is still limited by the beam splitter control noises as it is shown in Figure 27. These contributions have been estimated using the same analytical models as the one described in 4.2.2. The input bench resonances visible in the sensitivity curve between 30 and 60 Hz still propagate through the beam splitter longitudinal control loop. This loop also seems to introduce a large part of the noise in the 10-16 Hz region. The beam splitter θ_x angular control noise explains the sensitivity in both 22-34 Hz and 48-80Hz regions assuming a vertical miscentering of the incident beam with respect to the beam splitter mirror of 1.55 cm, which is exactly the same value as the one used for C4. This means that the coupling mechanism between the angular mirror displacement and the dark fringe signal did not change between the two runs.

5.4 Noise budget of the C5 run

The noise budget of the C5 run is presented in Figure 28. The sensitivity is limited by beam splitter control noises between 10 and 80 Hz, and by the electronic noise of the B1 photodiodes above 300 Hz. Between 80 Hz and 300 Hz the sensitivity is not fully understood. According to the measurement performed with no correction signal sent to the DAC, the actuator noise should not limit the sensitivity, but the hypothesis of the contribution of an additional non linear noise cannot be excluded.

6 Conclusion

Both C4 and C5 run analysis have shown that the recombined sensitivity was limited by beam splitter control noises in the low frequency part of the Virgo bandwith (below 100 Hz). The beam splitter longitudinal control loop is responsible for the propagation into the dark fringe signal of the input bench mechanical resonances which couple to the error signal $B2\_ACq$. This coupling can be reduced with a better tuning of the modulation

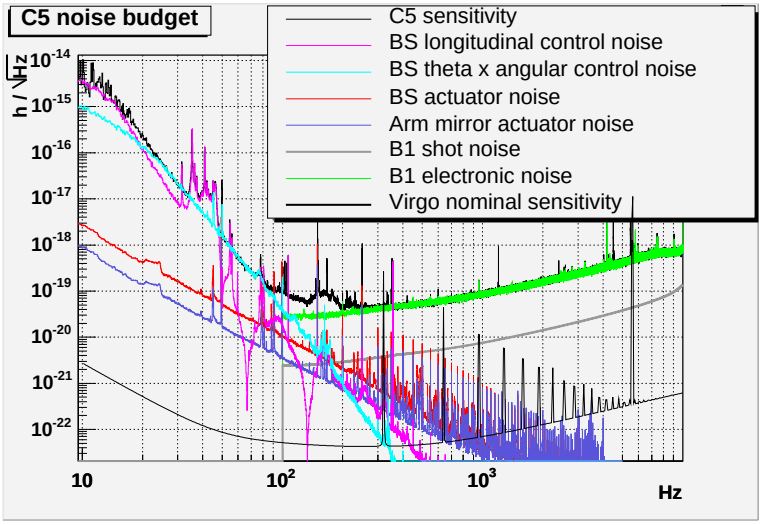

Figure 28: *Noise budget of the C5 run.*

frequency. The beam splitter angular local control has also been identified as a source of noise. A plausible hypothesis to explain the coupling mechanism between the beam splitter angular motion and the dark fringe signal is a vertical miscentering of the incident beam with respect to the beam splitter mirror. The required miscentering should be 1.5 cm.

The intermediate frequency region (70-300 Hz) was dominated by actuator noise during the C4 run. This analysis resulted in a technical upgrade of the actuator electronics which allowed the reduction of the contribution of this noise during the C5 run. Further improvements have been achieved since then in order to bring the actuator noise closer to the Virgo nominal sensitivity.

In the high frequency region (above a few hundred Hertz) the C4 run sensitivity has been shown to be essentially limited by the laser frequency noise induced by the electronic noise of the error signal $B2\_ACp$, whereas the C5 run sensitivity was limited by the dark fringe electronic noise. This difference is linked to the modification of the input bench optical setup which decreases the amount of power entering the interferometer. The contribution of these high frequency noises is reduced in recycled configuration.

References

[1] B. Caron et al., *A time domain, general purpose simulation program for the VIRGO experiment*, Astropart. Phys., 10/4, 369-386 (1999)

[2] L. Derome, *Le système de détection de l'expérience VIRGO dédiée à la recherche d'ondes gravitationnelles.*, Ph. D. thesis, University of Savoie (1999).

[3] F. Bondu, *Asymmetry in Virgo interferometer due to Perot-Fabry effect in corner mirrors: Analytical study.* (1996), Private communication.

[4] http://wwwcascina.virgo.infn.it/commissioning/OPC/Documents/ROC_measurement.pdf

[5] R. Gouaty, R. Flaminio, E. Tournefier, *Search for noise sources in C1 and C2 sensitivities*, Virgo Note VIR-NOT-LAP-1390-277 (2004).

[6] M. Laval, F. Bondu, JY. Vinet, *Optical simulation, mirror curvatures and long arms*, Virgo Note VIR-NOT-OCA-1390-300 (2005).

[7] F. Beauville, *Prélude à l'analyse des données du détecteur Virgo : De l'étalonnage à la recherche de coalescences binaires.*, Ph. D. thesis, University of Savoie (2005).

[8] R. Flaminio, *The effects of modulation frequency mismatch.*, ILIAS-GW N5-WP1 Meeting, http://www.ego-gw.it/ILIAS-GW/ (2005).

A Effect of an asymmetry between the two cavities in the recombined configuration

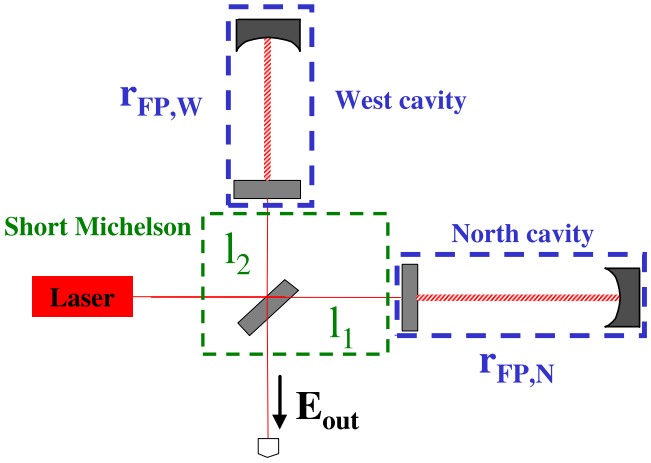

Figure 29: *Interferometer in the recombined configuration.*

The effect on the dark fringe signal of a difference between the complex reflectivities $r_{FP,N}$ and $r_{FP,W}$ of the two Fabry Perot cavities for the carrier is computed in the following.

The field E_{out} of the beam transmitted to the interferometer output port is the sum of three spectral components:

$$E_{out}(t) \;=\; A_0^t e^{i2\pi\nu_0 t} \;+\; A_+^t e^{i2\pi(\nu_0+\nu_{mod})t} \;+\; A_-^t e^{i2\pi(\nu_0-\nu_{mod})t} \tag{62}$$

where ν_0 is the frequency of the laser and ν_{mod} the modulation frequency, A_0^t is the amplitude of the carrier and A_-^t (respectively A_+^t) is the amplitude of the left (respectively right) side-band.
As it is demonstrated in [2] the amplitude of the carrier is given by:

$$A_0^t \;=\; -A_0 e^{i\frac{2\pi\nu_0 l_+}{c}} \Delta r \tag{63}$$

where:

- $\Delta r \ = \ \frac{r_{FP,W} - r_{FP,N}}{2}$. Δr is the difference between the reflectivities of the two cavities for the carrier.
- $l_+ \ = \ l_1 + l_2$. l_1 and l_2 are the short michelson lengths (as shown in Figure 29).
- $A_0 \ = \ J_0(m)A$. J_0 is a Bessel function, m is the modulation index, and A is the amplitude of the laser beam entering the interferometer.

The amplitudes of the side-bands are given by:

$$A^t_{\pm} \ = \ -A_{\pm} e^{i\frac{2\pi(\nu_0 \pm \nu_{mod})l_+}{c}} (\pm i) r_{bl} sin\Big(\frac{2\pi\nu_{mod} l_-}{c}\Big) \tag{64}$$

where:

- r_{bl} is the mean value of the reflectivities of the two Fabry Perot cavities for the side-bands. r_{bl} is assumed to be a real number because the side-bands are anti-resonant in the cavities.
- $l_- \ = \ l_2 - l_1$. l_- is the difference of length between the arms of the short Michelson.
- $A_{\pm} \ = \ \pm J_1(m)A$. J_1 is a Bessel function.

The power transmitted at the modulation frequency can be written as:

$$P_{mod} \ = \ \Big(A^t_+ \bar{A}^t_0 + A^t_0 \bar{A}^t_-\Big) e^{i2\pi\nu_{mod}t} \ + \ \Big(A^t_0 \bar{A}^t_+ + A^t_- \bar{A}^t_0\Big) e^{-i2\pi\nu_{mod}t} \tag{65}$$

By replacing the field amplitudes with their expressions (relations (63) and (64)) one obtains:

$$P_{mod} \ = \ 4A^2 J_0(m) J_1(m) \sqrt{T} Re(-i\Delta r) \ cos\left(2\pi\nu_{mod}\Big(t + \frac{l_+}{c}\Big)\right) \tag{66}$$

where $T \ = \ r^2_{bl} sin^2\Big(\frac{2\pi\nu_{mod} l_-}{c}\Big)$ is the transmission factor of the side-bands.
Finally, the signal S_p obtained after the demodulation process is:

$$S_p \ = \ 4A^2 J_0(m) J_1(m) \sqrt{T} Re(-i\Delta r) \tag{67}$$

Relation (67) shows that an asymmetry Δr between the complex reflectivities of the Fabry Perot cavities can generate a signal on the dark fringe.